SU-SEL-65-046

Studies of the Topside Ionosphere With the Alouette Satellite

by
T. M. Watt

April 1965

Technical Report No. 9

Prepared under
National Aeronautics and Space Administration
Grant 30-60

RADIOSCIENCE LABORATORY

STANFORD ELECTRONICS LABORATORIES

STANFORD UNIVERSITY • STANFORD, CALIFORNIA

SEL-65-046

STUDIES OF THE TOPSIDE IONOSPHERE WITH THE ALOUETTE SATELLITE

by

T. M. Watt

April 1965

Technical Report No. 9

prepared under
National Aeronautics and Space Administration Grant 30-60

Radioscience Laboratory
Stanford Electronics Laboratories
Stanford University Stanford, California

ABSTRACT

The aim of this research was to determine the electron temperature, ion temperature, and relative ion concentrations in the topside ionosphere, by using electron-density measurements obtained from the Alouette satellite.

Electron-density profiles obtained from Alouette soundings recorded at Stanford University provide the basis for scale-height profiles from which relative ion concentrations, electron temperatures, and ion temperatures can be deduced. Results are obtained for dip latitudes between 50 °N and 85 °N, and altitudes from 500 to 800 km.

The lower-latitude nighttime data can be interpreted adequately in terms of a three-constituent (O^+, He^+, H^+) diffusive-equilibrium model with an (O^+)-(He^+, H^+) transition occurring at about 600 km in the summer and 500 km in the winter. The transition level rises with increasing latitude, rising above 800 km at about 67 deg of dip latitude. The transition level also rises quickly at local sunrise and descends more slowly at local sunset. Scale heights for both summer and winter days vary only slightly with latitude but nighttime scale heights for both summer and winter have large latitudinal variations, which are interpreted in terms of latitudinal variations both in ion constituents and in electron and ion temperatures.

This analysis of scale height in a formal and detailed manner has, for the first time, brought out the following:

1. "Simple" analyses of scale heights in which isothermal or constant-gradient temperatures are assumed, can lead to serious errors in the interpretation of ion distributions.
2. In contrast with 1. above, analysis of scale-height profiles can lead to reasonable conclusions about temperature variations with both height and latitude--in particular, about ion temperature, heretofore a quantity not easily measured.
3. The existence of a transition from O^+ to lighter ions (i.e., He^+, H^+) is definitely established, and it is shown how the height of this transition varies with time and with latitude.
4. For the special case of a constant gradient of temperature with height, the relationship between a measured scale height and an arbitrary, nondivergent, upward flux of ionized particles is presented and it is shown how such an analysis may be extended to the case of an arbitrary temperature variation.

CONTENTS

TABLES

ILLUSTRATIONS

ILLUSTRATIONS (Cont)

LIST OF SYMBOLS

A, A_1, A_2, A_3	arbitrary constants
$\underline{A}$	matrix operator
B	geomagnetic field
$\underline{B}$	matrix operator
C	arbitrary constant
$\underline{C}$	matrix operator
D	diffusion coefficient
$\mathbb{D}$	differential operator
E	electric field
F	generalized force, arbitrary parameter
H	scale height
$\mathcal{H}$	plasma scale height
H^+	ionized hydrogen
He^+	ionized helium
I	dip angle
K	thermal conductivity
L	ionization loss rate per unit volume
M	equivalent mass
N	atomic nitrogen
N_2	molecular nitrogen
$N(h)$	electron density
O	atomic oxygen
O_2	molecular oxygen
P	relative concentration
Q	ionizing flux

R, S	arbitrary parameters
T	neutral temperature
T_e	electron temperature
T_i	ion temperature
W	vertical component of diffusion velocity
X, Y, Z	arbitrary atomic species
a, b	arbitrary parameters
a_r, a_γ	unit vectors
e	electronic charge, subscript referring to electron parameters
f	wave frequency
f_p	plasma frequency
g	acceleration of gravity
h	height coordinate
h'	virtual depth
i	subscript referring to ion parameters, also general summation index
j	subscript referring to a particular value of index i
k	Boltzmanns constant
m	mass
n	number density, matrix size
o	subscript referring to reference height value
p	pressure
q	production rate per unit volume
t	time
v	velocity
x	reduced height
z	height variable

Γ	scale height gradient
Φ	arbitrary constant
α	general exponential coefficient
α_e	dissociative recombination coefficient
β	general recombination coefficient
γ	ion-atom interchange coefficient
δ	dip latitude
ϵ	scale height gradient
ϵ_o	permittivity of free space
μ	refractive index
μ'	group refractive index
ν	collision frequency
τ	ratio of electron temperature to ion temperature
φ	angle between radial coordinate and equatorial plane
χ	zenith angle of sun
ω	radian frequency

ACKNOWLEDGMENT

The advice of Professor Owen K. Garriott, under whose guidance this work was performed, is very much appreciated. Also appreciated are the many helpful discussions which took place with Dr. J. O. Thomas and Professors O. G. Villard, Jr., and P. A. Sturrock.

The equipment maintenance as well as many of the data recordings were handled by Mr. S. C. Hall. A great amount of time was spent on data reduction by Mrs. Ulla Lundquist and Miss Jane Collins. The extensive programming required for obtaining electron-density profiles was performed by Dr. J. O. Thomas and other members of the Space Sciences Division of Ames Research Center. Without such a large amount of cooperation from these individuals and many unnamed members of this laboratory, this research could not have been completed.

Financial support for this work here has been provided by the National Aeronautics and Space Administration under Grant No. NsG 30-60.

I. INTRODUCTION

For many years the study of the ionosphere was limited to ground-based observations of electron-density phenomena. Since 1925, radio-pulse sounding has been used to study spatial and temporal characteristics of ionospheric electron density, and many important theories have been advanced explaining these observations. Ground-based radio sounding suffers from one major limitation, however--it provides information on electron density only up to the height at which electron density is at a maximum. Any radio signal that passes beyond this point in space is not reflected and thus provides no information.

The advent of rockets and then satellites has added a new dimension to the study of the ionosphere. Rocket-mounted instruments can make direct, if brief, measurements of parameters such as the relative concentrations of the various ion species and electron temperatures along the trajectory. Satellite-mounted instruments can perform comparable measurements over extended periods of time and wide distances, as well as many other types of measurements. At the same time, more advanced ground-based sounding schemes are being devised, and one of these--the incoherent-backscatter technique--has proved quite useful in the determination of electron and ion temperature variations in the ionosphere. All of these later methods permit the study of the region above the level of maximum ionization.

A major step forward took place in September 1962, when the Canadian Alouette satellite was launched. Mounted in the satellite was a radio sounder and, for the first time, direct sounding of the topside of the ionosphere was possible. The sounder has been operated and monitored on a routine basis since its launching and has proved to be a highly successful source of data.

As the satellite traverses its orbit, the sounder probes the region below, obtaining information about the distribution of electron density between the height of the satellite and the peak of the F_2 layer. The electron-density distribution may be interpreted in terms of the distribution of relative ion concentrations and electron and ion temperatures. In this research, I have been concerned with the study of these

distributions of temperature and relative concentrations, and their variations with height, latitude, local time, and season. In particular, I have considered data recorded at Stanford University during the periods May through July 1963 and November 1963 through January 1964. The results of about 80 satellite passages during these two periods, representing about 1200 separate soundings, have been analyzed. In general, the quality of the data has been excellent and has shown good consistency, thus permitting valuable conclusions to be drawn concerning ionospheric parameters.

A. DEFINITION OF THE PROBLEM

The aim of this research was to determine the electron temperature, ion temperature, and relative ion concentrations in the topside ionosphere, here loosely defined as the region between 500 and 800 km above the surface of the earth, by using electron-density measurements obtained from the Alouette satellite. To the author's knowledge, the technique here employed has never been used before to provide a detailed study of the above-mentioned quantities; it therefore deserves some explanation. These quantities have been studied by other techniques, and perhaps the best way to introduce this new method is to compare it with existing methods.

The rocket- or satellite-mounted electrostatic probe is a widely used method for determining local values for electron temperature and relative ion concentration. In principle, the method should provide values of ion temperature as well, although in practice this last parameter has proven difficult to determine accurately. Brace et al (1963, 1964)* have used this method quite successfully in determining profiles of electron temperature as a function of height and latitude. Many others, notably Bourdeau and Bauer (1962) and Bourdeau and Donley (1964), have studied spatial variations of electron temperature using the same technique.

Incoherent backscatter provides another method for determining electron temperature. In this method, energy is propagated into the ionosphere from an extremely powerful pulsed radar. One of the weaker echos received is due to scattering of waves from the individual electrons. The power returned is directly proportional to the electron density, and the

*See Bibliography.

width of the echo power spectrum is a function of the ratio of electron temperature to ion temperature (T_e/T_i). Unfortunately, the ratio is also a function of the ion mass, which must be determined independently or assumed; this is a major limitation of the backscatter method.

As noted above, the rocket- or satellite-mounted probe is also used to determine values of relative ion density. An outstanding example of this type of experiment is that of the U. K. satellite "Ariel" as reported by Bowen et al (1964).

All of these experiments represent "direct" methods. In each case the assumptions and approximations that must be made involve only local parameters; thus localized measurements lead to localized conclusions. Even in the incoherent-backscatter method, the specification of ion mass must be made only at the point where T_e/T_i is to be determined. This characteristic has the obvious advantage that a detailed knowledge of other parts of the ionosphere are not required; on the other hand, without such knowledge, detailed conclusions about other parts of the ionosphere cannot be made.

In contrast to these methods, I employed an "indirect" method for determining these quantities. As described in detail in Chapter V, the topside sounder provides an almost complete profile of electron density between the satellite and the height of the ionization maximum (the F-layer peak). The interval of time during which the sounder interrogates the region beneath the satellite for each sounding is only about 20 sec, and during this time the satellite travels approximately 100 km. Since under ordinary circumstances ionospheric time scales and spatial dimensions of interest are much greater than these, each electron-density profile may be considered to be a description of electron density as a function of height alone, commonly known as an $N(h)$ profile. It is well known that, at heights well above the peak of the F layer, electron density decreases with height in an <u>approximately</u> exponential manner--i.e.,

$$N(h) \approx N_o \exp[-\alpha(h-h_o)] \ . \qquad (1)$$

It turns out that the coefficient α is a function of electron temperature, ion temperature, and relative ion concentrations (or equivalently, mean ionic mass). The function α as used here is for symbolic purposes only; it will prove more fruitful to express the exponential coefficient in terms of a function known as scale height, which will be defined in a moment.

To separate these quantities, each of which is itself height-variable, a much more complete description of the ionosphere must be provided than was required for any of the direct measurements mentioned earlier. Because of the many complexities involved, I have made as many reasonable assumptions and approximations as possible. Dividends result from this "scale-height" analysis, however. Instead of being able merely to determine quantities along the satellite track, we can determine these quantities throughout the region of interest.

B. DEFINITIONS OF TERMS

It is useful to define several terms that appear frequently throughout this report. These terms are all in common use but occasionally are defined differently by different authors.

1. Dip Latitude

The latitude coordinates used are all north dip latitudes. These coordinates are determined by obtaining a world map of measured magnetic-dip angles and then, for each dip angle, defining a corresponding dip latitude by the relation

$$\tan \delta = \frac{1}{2} \tan I \ , \qquad (2)$$

where δ is dip latitude and I is dip angle. A brief discussion of dip latitudes and alternate coordinates is given by Onwumechilli (1964). A comparison of dip and geographic latitudes is shown in Fig. 1. Because of data limitations, I have considered only measurements made from 50-deg dip latitude to 85-deg dip latitude. Since the data exhibit significant changes within this region, I have differentiated the latitude range into two regions--a "midlatitude" region close to 50-deg dip latitude and a "high latitude" region close to 85-deg dip latitude.

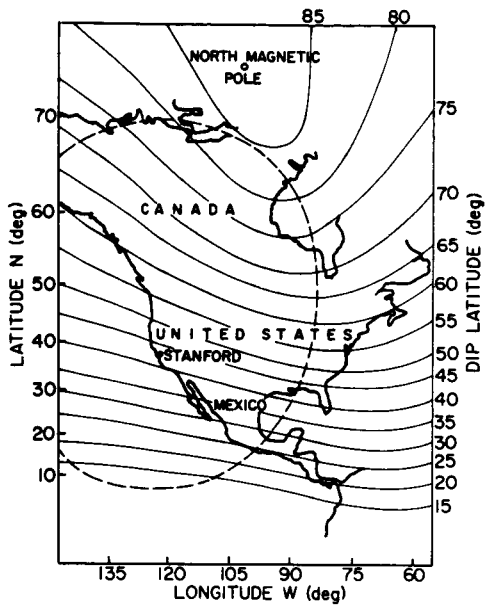

33206

FIG. 1. MAP SHOWING LINES OF CONSTANT DIP LATITUDE COMPARED WITH GEOGRAPHIC LATITUDE. Approximate limits of data acquisition from the Alouette satellite are indicated.

The choice of dip latitude as a coordinate is, to some extent, arbitrary. It was felt that magnetic coordinates of some kind were needed if longitudinal variations in the data were to be neglected. The computer program for reducing ionograms to $N(h)$ profiles described the satellite position in terms of both dip angle and dip latitude. The use of some other magnetic coordinate system such as that developed by McIlwain (1961) would not have been of any particular advantage in this study since I do not attempt to relate phenomena along field lines.

2. Scale Height

The term "scale height" was introduced and defined in 1931 by Chapman, using the expression

$$H = -\left[\frac{\partial}{\partial h}(\ln p)\right]^{-1} = \frac{-p}{\partial p/\partial h} \qquad (3)$$

in which h is height and p is pressure. As defined, it was a measure of the rate at which atmospheric pressure decreased with height. Alternatively, many authors today define scale height by the relation

$$H = \frac{kT}{mg} \tag{4}$$

for neutral species, and

$$H = \frac{k(T_e + T_i)}{2mg} \tag{5}$$

for an ionized species, where k is Boltzman's constant, T, T_e, and T_i are temperatures of neutrals, electrons, and ions respectively, m is the atomic mass of the species under consideration, and g is the acceleration of gravity. The two alternative definitions are approximately the same and, under the assumption of equal electron and ion temperatures and a uniform gravitational field, they are identical. Analogous to Chapman's definition, I define a term that is a measure of the rate at which electron density decreases with height in the topside ionosphere--"plasma scale height" or simply "scale height" for short--symbolize it with a script letter, and define it by the relation

$$\mathscr{H} = -\left[\frac{\partial}{\partial h}(\ln n_e)\right]^{-1} = -\frac{n_e}{\partial n_e / \partial h} \tag{6}$$

in which n_e is electron-number density. The quantity $\mathscr{H}$ is useful because it is an experimentally measurable quantity. Virtually the entire content of this report is devoted to the interpretation of theoretical and experimental values for $\mathscr{H}$. The quantity H as expressed in Eq. (5) is considered only as an index of the quantities T_e and T_i. The term "scale height" is interpreted only in terms of the definition given in Eq. (6). Using relations equivalent to Eqs. (5) and (6), many authors make the statement that $\mathscr{H} = 2H$, but this is true only in the special case when T_e, T_i, and g are all independent of height.

II. DESCRIPTION OF THE IONOSPHERE

Before a definitive relationship can be established between scale height and the quantities of interest, a relationship must first be established between the various processes in the ionosphere and the distribution of the different species of charged particles. To this end, I consider what are generally believed to be the important processes in the ionosphere and the regions in which certain of these processes dominate others insofar as they affect the distribution of ionization.

A. PHYSICAL PROCESSES IN THE IONOSPHERE

There are three basic processes in the ionosphere--production, loss, and transport. They are related by the equation of continuity; i.e.,

$$\frac{\partial n}{\partial t} + \nabla\cdot(n\bar{v}) = q - L \quad , \tag{7}$$

where n refers to number density, q to a production rate per unit volume, L to a loss rate per unit volume, and $\bar{v}$ is some average velocity associated with a particular species. The quantity $n\bar{v}$ thus defines a flux of particles--that is, the number of particles flowing across a unit area in unit time. The equation of continuity is essentially a bookkeeping operating, in that it accounts for the net gain or loss of a species (or any number of species for that matter) by all conceivable means in some arbitrary volume in space. It is thus satisfied everywhere in space. It may turn out, however, that under certain conditions one or more of the terms may become quite small in comparison to the others; the equation thus becomes simpler.

Observations and measurements of the ionosphere for many years have lead to the conclusion that, except at sunrise and sunset, the ionospheric processes are usually in approximate equilibrium. Significant exceptions exist, of course, such as eclipse effects and local enhancement of ionization due to meteors, etc. For studies such as this, however, in which data over several hours or days are averaged, it is usually considered a reasonable approximation that $\partial n/\partial t$ is much smaller than the other terms

and may be neglected. Under these conditions, then, Eq. (7) may be expressed as:

$$\nabla\cdot(n\bar{v}) = q - L \ . \tag{8}$$

Each of the remaining terms can now be investigated separately.

1. Production Processes

There are two important production processes--solar ionization and corpuscular ionization. Solar ionization results from the absorption of solar ultraviolet (uv) and X-ray radiation. This absorption is considered to be the principle production process, at least at low or medium latitudes. Corpuscular ionization, which is ionization resulting from collisions between higher-energy charged particles and atmospheric constituents, is believed to be most significant at high latitudes and during magnetic storms. The source of these particles is considered to be probably the solar wind and/or the Van Allen belts.

The importance of corpuscular ionization has not been fully established and is presently the subject of a great deal of study. A detailed study of ion production would be very tedious but a first-order description can be obtained by considering Chapman's theory (Chapman, 1931). The Chapman theory considers a monochromatic source of solar radiation impinging on a flat earth whose atmospheric number density varies as $\exp[-h/H]$, where H is given by Eq. (4). The radiation intensity decreases downward as it is absorbed by the atmosphere. The production function q at any point is proportional to the product of the radiation intensity and the gas number density, resulting in a peak of production occurring at some height. The exact expression is given by

$$q(h) = q_o \exp\left\{1 - \frac{1}{H}(h-h_o) - \exp\left[-\frac{1}{H}(h-h_o)\right]\right\} \ , \tag{9}$$

in which h_o is the height of peak production. Now, in fact, the earth is not flat, solar radiation is not monochromatic, and H is not a constant; nevertheless, Eq. (9) is considered to be a first-order approximation

to reality. In particular, note that, for $h-h_o \gg H$, Eq. (9) reduces to

$$q(h) \approx q_o \exp\left[-\frac{1}{H}(h-h_o)\right]. \tag{10}$$

2. Loss Processes

It is generally believed that, above about 200-km height, the principal loss process is ion-atom interchange followed by dissociative recombination (Bates and Massey, 1947). Symbolically,

1. Ion-atom interchange (coefficient γ)

$$X^+ + YZ \rightarrow XY^+ + Z$$

2. Dissociative recombination (coefficient α_e)

$$XY^+ + e \rightarrow X^* + Y^* .$$

It is believed that the coefficient α_e is sufficiently large so that reaction 2. occurs more rapidly than 1., and therefore the total reaction is limited by the coefficient γ (Bates, 1955). The appropriate loss term, as applied to Eq. (8), is then given by the coefficient γ times the product of the respective number densities of ion species X^+ and molecular species YZ; i.e.,

$$L \approx \gamma\, n(YZ)\, n(X^+) = \beta\, n(X^+) \tag{13}$$

where the coefficient β depends on the ion species and the number density and species of the molecule. It is generally believed that the ionizable gas is atomic oxygen (hence $X^+ = O^+$) and the molecule involved in the reaction is either N_2 or O_2.

From ground level up to about 100 km, the neutral constituents of the atmosphere are well mixed because of turbulence. Above this level, however, it is believed that the number densities vary independently according to Dalton's law of partial pressures, and that the gases are

diffusively separated. Thus β varies approximately as

$$\beta \propto \exp\left[-\frac{h}{H(XY)}\right], \tag{14}$$

where $H(XY)$ is given by Eq. (4), appropriate for species XY.

3. Transport Processes

The main transport systems in the ionosphere are convection, (ambipolar) diffusion, and electromagnetic drift. Convection arises from motions of the neutral atmosphere that may carry the ionized gas with it. Diffusion arises from density gradients in the ionized gas that cause the ions and electrons to diffuse away from the region of high concentration. Unequal gradients among different species can cause them to diffuse among each other as well. Electromagnetic drift arises from the existence of an electric field perpendicular to the geomagnetic field, giving rise to the drift velocity $\bar{v} = \bar{E} \times \bar{B}/B^2$. Except for localized phenomena, convection is considered to be of less importance than diffusion, so will not be examined further.

Quinn and Nisbet (1965) and others have shown that drift velocity and diffusion velocity are probably of comparable magnitude near the F-region peak, and that drift velocity varies slowly with altitude while diffusion velocity increases approximately as $1/n(X^+)$ above the peak. Thus, even a short distance above the peak, diffusion velocity is probably much larger than drift velocity. In the region well above the F_2 peak, then, electromagnetic drift is also believed to be of less importance than diffusion and will not be considered further.

At sufficiently high altitudes, where collision frequencies are much smaller than gyro frequencies, it is a good approximation that ionized particles are constrained to travel along geomagnetic-field lines. Ratcliff (1960) has compiled a large number of experimental results suggesting that such an approximation is reasonable as low as 200 km. In regions where the dip angle is large, the component of travel in the horizontal direction is much smaller than the component in the vertical direction. In addition, observed values of number densities, temperatures, and radiation intensities have shown much smaller horizontal gradients than vertical

gradients. Thus horizontal fluxes of ionized particles would not affect vertical distributions.

A particular exception may exist at the times of local sunrise and sunset. A region of the ionosphere just emerging into sunrise might experience a large local gradient of ionization from the dark side to the light side. The importance of this phenomenon has not been clearly established. It is known, as noted previously, that processes are not in equilibrium at sunrise and sunset. With this exception in mind the transport term in the continuity equation can be expressed as

$$\nabla\cdot(n\bar{v}) \approx \frac{\partial}{\partial h}(nW) \tag{15}$$

in which W is the vertical component of $\bar{v}$. In view of the earlier consideration of transport processes, Eq. (15) indicates that the transport phenomenon of interest is a diffusive flux of ionized particles in a vertical direction. In the region of interest, (i.e., below 1000 km) the level of ionization is very low, at most a few percent. In this situation it is reasonable to assume that the diffusion of the charged particles through the meutral gas has very little effect on the neutral distribution. At the same time, the effect of the fixed neutrals on the particular species may be approximated by a viscous drag force that is of the form $nm\,\nu\,W$, where ν is the charged-particle - neutral collision frequency. Shimazaki (1959) has shown that under these conditions the transport term may be expressed as

$$\frac{\partial}{\partial h}(nW) = D\,\mathbb{D}(n)\ , \tag{16}$$

in which D is the diffusion coefficient and $\mathbb{D}$ is a differential operator. The evaluation of $\mathbb{D}$ in the general case is fairly complicated, but is of the form

$$\mathbb{D}(n) = A_1\frac{\partial^2 n}{\partial h^2} + A_2\frac{\partial n}{\partial h} + A_3 n \tag{17}$$

where A_1, A_2 and A_3 are functions of temperature but not of collision frequency. Of greater immediate interest is the diffusion coefficient D. In Chapter VIII, D is shown to be inversely proportional to ν. Simple gas kinetic theory shows that ν is directly proportional to the neutral density. Analogous to Eq. (14), D varies approximately as

$$D \propto \exp\left[\frac{h}{H}\right] . \tag{18}$$

In Chapter VIII I describe a more rigorous analysis of Eq. (16), but, for the present, these approximate arguments are sufficient. The relative importance of the three processes--production, loss, and transport--can now be compared.

Early workers in this field, using ground-based techniques, did not consider diffusion to be important, so their equilibrium-continuity equations were of the form $q \approx L$. Substituting for L from Eq. (13) gives

$$n(X^+) \approx q/\beta . \tag{19}$$

This expression agrees reasonably well with measurements of electron density between about 200 and 300 km. Equation (19) is unable to explain the existence of a peak, or maximum, of electron density, with a decreasing density above that level. For heights well above the peak of <u>production</u> (not the same as the peak of electron density), it follows, from Eqs. (10) and (14), that

$$n(X^+) \propto \exp\left\{\left[\frac{1}{H(XY)} - \frac{1}{H(X)}\right] h\right\}. \tag{20}$$

From the definition given in Eq. (4) it is apparent that $1/H(XY) = m(YZ)g/kT$ and $1/H(X) = m(X)g/kT$; thus if X refers to O and YZ refers either to O_2 or N_2, then $1/H(XY) > 1/H(X)$ always, and $n(X^+)$ increases monotonically with altitude. Equation (19) thus breaks down at high altitudes.

The importance of diffusion was suggested by Hulburt (1928), and the mathematical expressions were derived by Ferraro (1945). Yonezawa (1956)

showed that diffusion could provide an explanation for the existence of the F_2 peak. From the simple arguments just given it is clear that, as height increases, q and L become arbitrarily small, D becomes arbitrarily large, and diffusion must eventually become the dominant process, with the result that the continuity equation reduces to

$$\mathbb{D}(n) = 0 \ . \tag{21}$$

It is now generally believed that: 1) well below the F_2 peak, production and loss dominate; 2) well above the F_2 peak, diffusion dominates; and 3) the F_2 peak itself represents a region in which production, loss, and diffusion are of comparable importance. These regions well below and well above the peak are sometimes known as the "photochemical" regime and the "diffusive-equilibrium" regime, respectively. The term diffusive equilibrium may not be an ideal description, since it implies that the region is in perpetual equilibrium, which as already mentioned, may not be true at sunrise and sunset. Nevertheless, if these periods are avoided in this analysis, it is reasonable to state that the region is in "quasi-equilibrium" and that this equilibrium is maintained by the process of diffusion.

The height above which Eq. (21) may be considered valid has not yet been established; it has only been noted that it is somewhere above the F_2 peak. To determine this height, it is necessary to examine some aspects of the morphology of the ionosphere in terms of known distributions of different particle species.

B. MORPHOLOGY OF THE IONOSPHERE

It is instructive to consider the variations of the number densities of the various constituents with respect to spatial coordinates. The constituents can be classified in three categories--as neutrals, electrons, and ions--and can be treated individually.

1. Neutral Distribution

Up to about 100-km height the neutral atmosphere is believed to be turbulent and well mixed, composed mainly of N_2 and O_2 with small quantities of other gases. Above this level, known as the turbopause, the

constituents tend to separate diffusively. In addition, as pointed out by Nicolet and Mange (1954), O_2 tends to become increasingly dissociated into atomic oxygen with increasing height. The reverse reaction, association, proceeds slowly enough so that O, O_2, and N_2 tend to separate diffusively. Experimental evidence by workers such as Schaefer and Brown (1964) and Nier et al (1964) confirms this hypothesis. The results of Nier et al indicate that O is the dominant neutral constituent above 200 km.

2. Electron-Number Density

At midlatitudes, the peak of the $N(h)$ profile moves up and down diurnally from about 275 km in the daytime to about 350 - 375 km at night. The magnitude of the maximum electron-number density also decreases at night. The transition from a daytime condition to a nighttime condition seems to take place within two hours or so, and there has been a great deal of speculation as to why the nighttime ionosphere does not continue to decay. At heights greater than about 150 km above the peak, the $N(h)$ profile varies approximately as a decreasing exponential.

Many workers have actively studied the variation of electron-number density with latitude, but the phenomenon is not yet well understood. Variations of electron density with latitude reveal peculiar enhancements and depletions of ionization both near the magnetic equator and near the auroral zones. It is thought that the depletion of electron density near the magnetic equator, known as the "equatorial anomaly", might be due to the very shallow dip angle which would tend to inhibit vertical diffusion and enhance latitudinal diffusion. At the high latitudes, Thomas (1963) has observed a marked enhancement of ionization, apparently occurring only in the winter hemisphere.

Finally, theoretical studies and experimental results of satellite drag measurements (O'Sullivan et al, 1963), have led to reasonable estimates of neutral-number density as a function of height. Comparing these numbers with observed values of electron-number density allows us to conclude beyond doubt that in the region, say, below 1000 km, the ionosphere is a weakly ionized gas, with not more than a few percent of the particles ionized.

3. Ion Constituents

It is believed that the most abundant ions in the upper ionosphere are O^+, He^+, and H^+. There is little doubt that O^+ is the dominant ion at least between 200 and 500 km. Ion-mass-spectrometer measurements (Johnson et al, 1958) plus the knowledge that atomic oxygen is abundant in this region, make this a virtual certainty. At altitudes above about 1500 km it is generally believed that H^+ is the dominant ion. Recent measurements of hybrid resonances at 1000 km by Barrington et al (1964) suggest comparable ratios of H^+ to O^+ at this altitude. On the other hand, the relative abundance of He^+ in the ionosphere is not yet fully established. Nicolet (1961) suggested that helium might be an important constituent of the upper atmosphere. King et al (1964) present experimental results suggesting an O^+ to He^+ transition at about 600 km. Bowen et al (1964) show experimental results indicating that He^+ is a dominant ion at 800 km, with O^+ and H^+ also present in significant quantities. Their results appear to disagree to some extent with those of Barrington et al, so the matter cannot be considered as completely settled. It does seem apparent, however, that if other ions are present in the upper ionosphere, they are in minor proportion to O^+, He^+, and H^+.

4. Scale Height

Typical scale-height profiles reduced from $N(h)$ profiles exhibit a consistent characteristic that is of great importance here. Starting at altitudes well above the F_2 peak and moving downward, scale height always decreases with decreasing height until within about 100 km of the F_2 peak. Closer to the peak, scale height increases sharply and becomes infinite at the peak itself. This sudden increase of scale height in the vicinity of the peak not only signals the imminence of the F_2 peak, but also serves as a sensitive indication that the $N(h)$ profile is deviating from an approximate exponential. I make use of this property in considering the interpretation of the data from the Alouette satellite.

C. USEFUL APPROXIMATIONS

From the description of the ionosphere given thus far, the stated and implied approximations that will be useful in this study can be summarized and qualified.

It was stated earlier that the importance of production and loss diminished with altitude and the importance of diffusion increased with altitude. Above some arbitrary altitude, then, the assumption that the ionosphere is in a state of diffusive equilibrium (again, assuming $\partial n/\partial t \approx 0$) is valid. A reasonable estimate of this arbitrary altitude can be determined in the following manner. It is shown in Chapters IV and VIII that electron-density distribution solutions are always exponentials in height for the case of diffusive equilibrium. In the discussion of scale height, above, it was noted that, from high above the peak of ionization, scale height decreases slowly with decreasing height and then suddenly increases and becomes infinite. This sudden increase of scale height will be used here to determine the lower boundary of the diffusive equilibrium regime. Most workers in this area consider a height of 500 km as a reasonable boundary; my own analysis supports this value.

Assume that in any small region of space, electrons are in temperature equilibrium, neutrals are in temperature equilibrium, and all ions are in temperature equilibrium (i.e., all ion species have the same temperature). These assumptions are necessary if the concept of temperature is to be meaningful. Thus assume that, at any height, the ions O^+, He^+, and H^+ are in temperature equilibrium. This is a reasonable assumption since Evans and Loewenthal (1964) have observed that electron and ion temperatures reach approximate equilibrium in a matter of 1 to 2 hours after sunset. The equilibrium of the temperatures of, say, O^+ and H^+ should occur much more rapidly since their masses are much more nearly equal. It does not follow, however, that electrons, ions, and neutrals are necessarily in equilibrium with each other in general. Hanson (1962) and Dalgarno and McElroy (1963) studied this problem for the case of a continuous influx of ionizing energy. The results of Hanson's study are examined in greater detail in Chapter III.

The approximations that have been justified thus far are stated below.

1. $\partial n/\partial t = 0$ except at sunrise and sunset.
2. $q = L = 0$ above 500 km.
3. Horizontal gradients of all quantities are much smaller than vertical gradients and thus may be neglected.
4. Only the vertical component of flux of ionized particles are considered. Horizontal fluxes of ionized particles and all fluxes of neutral particles are ignored.
5. At any point in space, all ions have the same temperature.
6. The region above 500 km is composed entirely of a statistically neutral mixture of electrons and H^+, He^+, and O^+ ions, along with neutral particles, and this mixture is in diffusive equilibrium.

III. OTHER EXPERIMENTAL AND THEORETICAL WORK

In the past three years a great deal of experimental and theoretical work has been done by many workers in an attempt to determine more clearly the distribution of the various ion species and the variations of electron and ion temperatures. The results thus far are sketchy and incomplete and are therefore not classified under Chapter II. Some of the results of this work can be considered quantitatively and in some cases these results can be used as boundaries for the present research.

A. THEORETICAL ION DISTRIBUTIONS

The earliest known theoretical work in this area was that of Mange (1960), who considered a diffusive equilibrium mixture of O^+ and He^+ ions for the case in which electron temperature, ion temperature, and the gravitational field were all independent of height. Since that time, other workers have considered the problem, the latest effort being that of Angerami and Thomas (1964), who consider a ternary (O^+, He^+, H^+) mixture in diffusive equilibrium for heights above 500 km. They consider heights out to several earth radii at all latitudes for the case in which there is no net velocity associated with any species, and T_e/T_i is a constant along any geomagnetic-field line.

B. THEORETICAL TEMPERATURE PROFILES

Dalgarno et al (1962) and Hanson (1962), using different approaches, present theoretical studies of temperature distributions in a daytime atmosphere in which the energy input is electron heating by extreme ultraviolet flux, and energy transfer occurs through a variety of collision mechanisms. Some of their results are important to the present study and are summarized here.

1. Above 300 km the predominant heavy particles are O^+ ions and, unless electron temperatures are extremely high, collisions with neutral particles may be ignored. The primary collision process is therefore electron-ion coulomb interaction.

2. Under the conditions governed by 1, the rate of electron-ion energy transfer is given by

$$\left(\frac{dT_e}{dt}\right)_{O^+} = - \frac{n_e\left(T_e - T_i\right)}{268\ T_e^{3/2}} \quad , \tag{22}$$

where n_e is given in cm^{-3}.

3. If Q is the input heat flux to the electron gas, then, in equilibrium,

$$\frac{dT_e}{dt} = 0 = Q - \frac{3\ k\ n_e}{2}\left(\frac{dT_e}{dt}\right)_{O^+} . \tag{23}$$

Combining Eqs. (22) and (23) yields

$$T_e - T_i = \frac{2.1 \times 10^6\ Q\ T_e^{3/2}}{n_e^2}\ ^\circ K \ , \tag{24}$$

where Q is expressed in ev/cm^2-sec. Using a simple exponential variation of electron density of the form $\exp[-h/H]$ where $H = k(T_e + T_i)/mg$, and considering an idealized case of all energy input taking place below some arbitrary reference level, Hanson derives the result

$$Q\ H \approx - K \frac{dT_e}{dh} \quad , \tag{25}$$

where K is the thermal conductivity of the plasma along the field lines. A value of K is given by Hanson as

$$K = 7.7 \times 10^5\ T_e^{5/2}\ ev/sec\text{-}cm\text{-}^\circ K \ , \tag{26}$$

Using this value for K, typical values $T_e = 1800\ ^\circ K$ and $T_i = 1400\ ^\circ K$, and substituting for Q from Eq. (24) leads to

$$\frac{dT_e}{dh} = -\ 4.8 \times 10^{-11}\ n_e^2 \quad \text{deg/km} \ . \tag{27}$$

For altitudes greater than 500 km, equilibrium electron densities are typically less than 10^5 per cm^3; thus the gradient expressed by Eq. (27) is typically less than 1 deg/km.

Finally, Hanson shows that, with increasing altitude, collisions between ions and neutrals become less frequent and, in the region between 500 km and 800 km altitude, ion temperatures increase with height from the lower neutral temperature to the higher electron temperature.

C. EXPERIMENTAL ION DISTRIBUTIONS

The primary sources of information available on topside ionosphere ion distributions are satellite-mounted mass spectrometers. Results obtained from Explorer VIII have been discussed by Bourdeau and Bauer (1962) and Bourdeau and Donley (1963). Results of the Ariel satellite are discussed by Bowen et al (1963). Both satellites carried mass spectrometers and the experiments were similar in many respects. The Ariel experiment yielded data for the summer of 1963 and within the latitude range of the present study, so it is considered here.

The Ariel satellite orbited at an average height of about 800 km, and relative concentrations of ions H^+, He^+, and O^+ were obtained along the satellite track. The published results are in terms of "transition heights"--that is, heights corresponding to equal concentrations of O^+ and He^+ and equal concentrations of He^+ and H^+. Two sets of curves are presented, corresponding to <u>geographic</u> latitudes of -10 to + 10 deg and 35 to 45 deg. The curves for the midlatitudes (35 - 45 deg) are shown in Fig. 2. The transition heights are determined by extrapolating the direct measurements upward and downward on the assumption that T_e, T_i, and g are independent of height and the medium is in diffusive equilibrium. Their assumptions about T_e, T_i, and g are, strictly

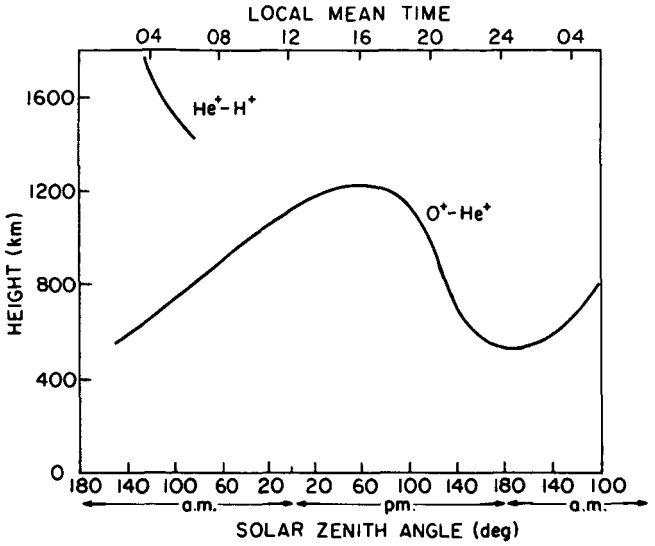

33215

FIG. 2. TRANSITION LEVELS FROM THE ARIEL SATELLITE. Upper curve is He^+-H^+ transition; lower curve is O^+-He^+ transition. Curves represent an average of data obtained at 35° to 45° North geographic latitude. (From Bowen et al, 1964.)

speaking, not in keeping with those made in the present study. Although ion-concentration data at the satellite height is not explicitly stated in Bowen's paper, the information is easily obtained from a knowledge of the predicted transition levels.

The equations used by Bowen to determine transition levels are

$$T = 1340 + 295 \cos\left[\frac{2\pi}{24}\,(1400 - \mathrm{LMT})\right] \tag{28}$$

and

$$h = \frac{-2.303\ kT}{[m(O^+) - m(He^+)]\ g} \log \frac{n(He^+)}{n(O^+)} + h_o\ . \tag{29}$$

Equation (28) expresses the assumption that the diurnal variation of temperature is sinusoidal, with a maximum occurring at 1400 LMT (local mean time) and a minimum at 0200 LMT.

Equation (29) expresses transition height h in terms of a known concentration ratio at height h_o. The force of gravity is considered

constant. Equation (29) may be restated as

$$\frac{n(He^+)}{n(O^+)} = \exp\left[\frac{(h_o - h_1)\,[m(O^+) - m(He^+)]\,g}{kT}\right]. \qquad (30)$$

from which it follows that

$$\frac{n(H^+)}{n(He^+)} = \exp\left[\frac{(h_o - h_2)\,[m(H^+) - m(He^+)]\,g}{kT}\right]. \qquad (31)$$

Referring to Fig. 2, use a typical local time of 0200, for which the mid-latitude transition levels are taken as 600 km for O^+-He^+ and 1800 km for He^+-H^+. If 800 km is taken as an average altitude of the Ariel satellite, then by use of Eqs. (28), (30), and (31), we can solve for the ion concentrations that were apparently measured by the satellite at 800 km.

From Eq. (28),

$$T = 1045\ ^\circ K\ . \qquad (32)$$

The gravitational field at 700 km is

$$g(700) = g_1 = 7.96\ m/sec^2\ . \qquad (33)$$

The gravitational field at 1300 km is

$$g(1300) = g_2 = 6.76\ m/sec^2\ . \qquad (34)$$

Using these values of g_1 and g_2 in Eqs. (30) and (31) respectively results in

$$\frac{n(He^+)}{n(O^+)} = 9.0 \qquad (35)$$

and

$$\frac{n(He^+)}{n(H^+)} = 10.4 \ . \tag{36}$$

Relative concentration of O^+ is found as

$$P(O^+) = \frac{100 \times [n(O^+)/n(He^+)]}{[n(O^+)/n(He^+)] + [n(H^+)/n(He^+)] + 1} = 9 \text{ percent} \ . \tag{37}$$

Similarly,

$$P(He^+) = 83 \text{ percent} \tag{38}$$

and

$$P(H^+) = 8 \text{ percent} \ . \tag{39}$$

Equations (37), (38), and (39) give relative concentrations of the three constituents that should be reasonably close to the values actually measured at 0200 LMT and at a height of 800 km. Later, I will compare these values with values predicted by my own theoretical model. It should be noted that the relative concentrations listed above are good approximations to "raw" data and as such are not restricted by the assumptions expressed in Eqs. (28) and (29).

D. EXPERIMENTAL TEMPERATURE PROFILES

Evans and Loewenthal (1964), using backscatter techniques, obtained values for T_e/T_i, as shown in Figs. 3, 4, and 5, representing data taken in July 1963 at Millstone Hill Observatory (58-deg dip latitude). Determination of the values shown in Figs. 3 and 4 is based on the assumption that O^+ is the only ion present, and the effect of such an assumption is shown in Fig. 5.

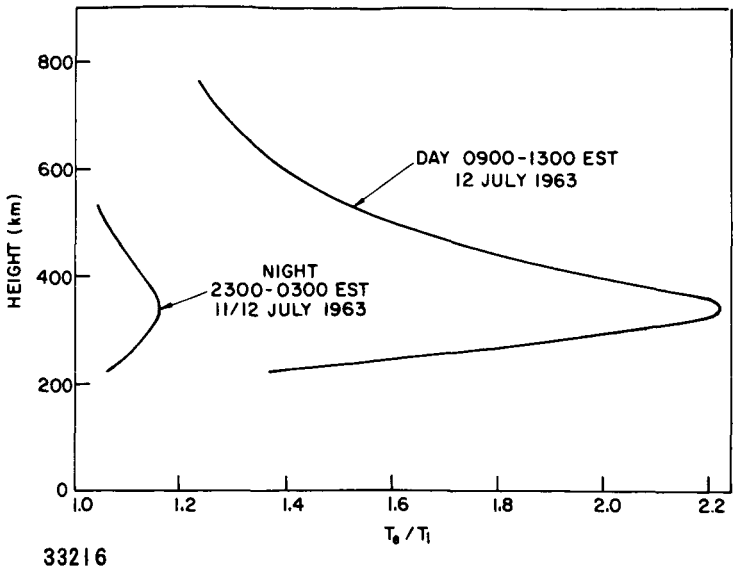

33216

FIG. 3. SUMMER DAYTIME AND NIGHTTIME VALUES OF T_e/T_i AT 58-DEG DIP LATITUDE. Data obtained by backscatter techniques. (From Bowen et al, 1964.)

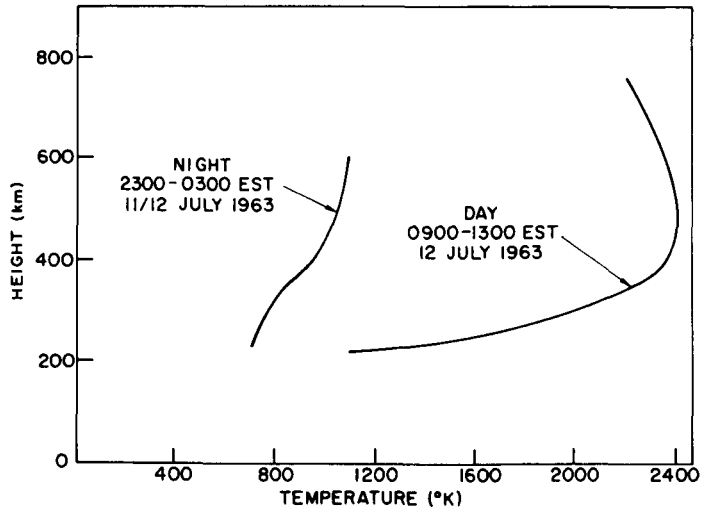

33217

FIG. 4. SUMMER DAYTIME AND NIGHTTIME VALUES OF ELECTRON TEMPERATURE AT 58-DEG DIP LATITUDE. Data obtained by backscatter techniques. (From Evans and Loewenthal, 1964.)

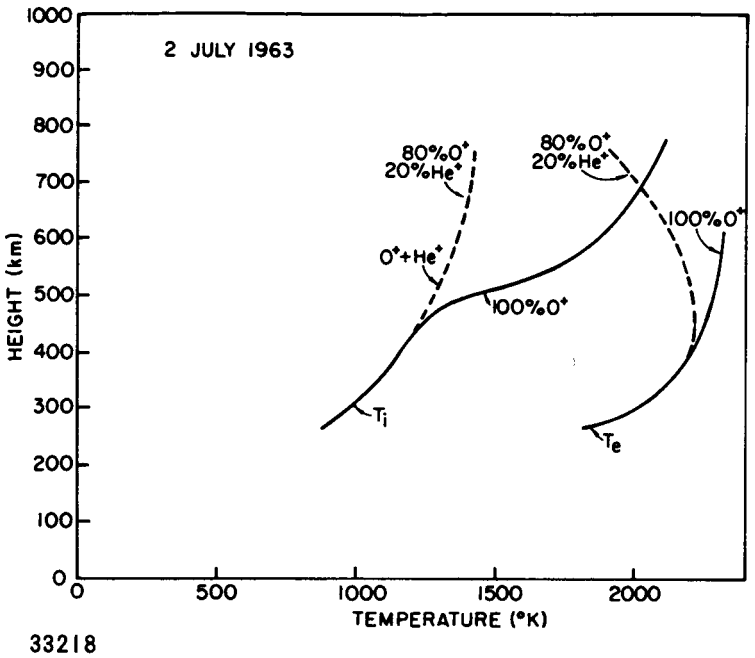

FIG. 5. SUMMER DAYTIME ELECTRON AND ION TEMPERATURES AS FUNCTIONS OF HEIGHT. Effect of different assumptions about relative ion concentration is shown. Data obtained at 58-deg dip latitude by backscatter techniques. (From Evans and Loewenthal, 1964.)

Brace et al (1963), reporting on the results of several rocket-mounted ionospheric probes, obtained the results shown in Fig. 6, in which data from Wallops Island, Virginia (52-deg dip latitude) and Fort Churchill, Canada (72-deg dip latitude) are considered. The data suggest that, for heights greater than 300 km, 1) electron temperatures at midlatitudes tend to be independent of height both at night and in the daytime, and 2) electron temperatures tend to increase with increasing latitude, at least during the day. The observation that electron temperatures increase with increasing latitude has been reported by many workers--Bowen et al (1964), Brace and Spencer (1964). Daytime latitude variations of electron temperatures are linked to observed electron-density measurements through relations such as Eq. (24), where Q is assumed to vary with latitude as $\cos \chi$ (χ = zenith angle of the sun). The reports in general are not quantitative, noting only that the latitudinal variation of electron temperature agrees with observations of electron-density variations. It seems likely that detailed latitudinal data have not been available heretofore, thus making quantitative conclusions difficult to obtain.

Nighttime electron temperatures have also been observed to increase with increasing latitude, although again detailed data appear to have

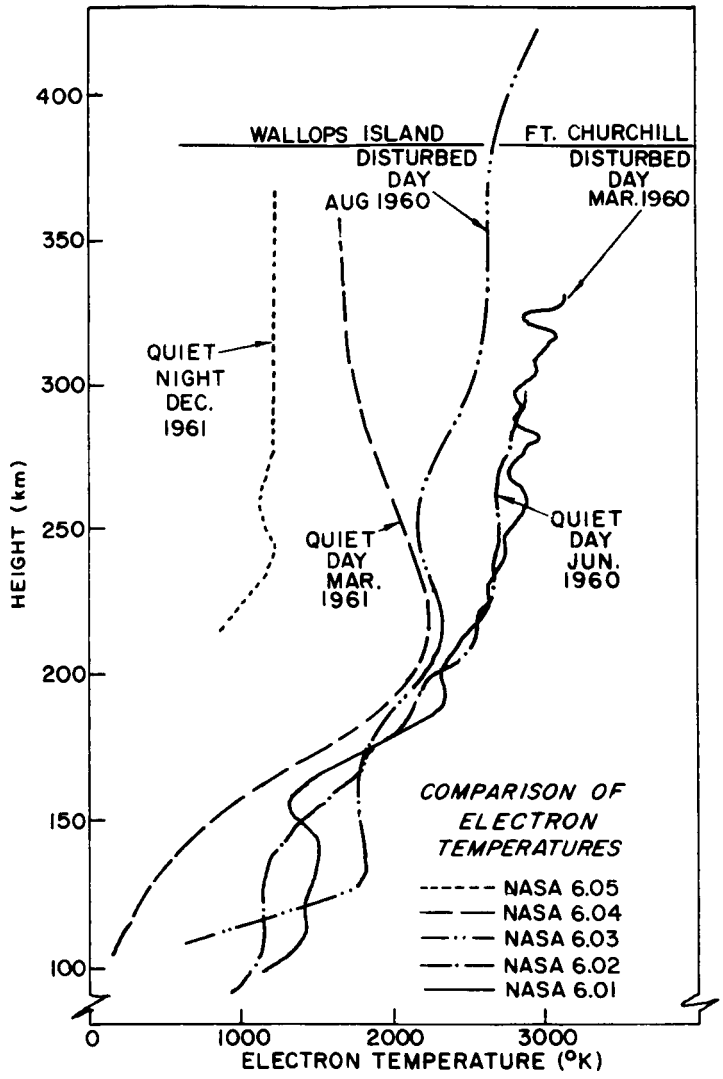

FIG. 6. ELECTRON TEMPERATURES FOR DAYTIME AND NIGHTTIME CONDITIONS. Data obtained from rocket-mounted probes. The curves show that electron temperatures tend both to: 1) be isothermal above 300 km and 2) increase with increasing latitude. Wallops Island is at 52-deg dip latitude; Fort Churchill is at 72-deg dip latitude. (From Brace et al, 1963.)

been lacking up to now. There has been speculation that this increase in temperature may be caused by energy sources such as particle precipitation, but aside from that, no conclusions are available.

IV. METHOD OF SOLUTION

A. DESCRIPTION OF ASSUMPTIONS AND APPROXIMATIONS

Three categories of assumptions and approximations are made in this study:

1. Those based on the physics and morphology arguments of Chapter II
2. Those based on the experimental evidence of Chapter III
3. Those required to make certain expressions tractable.

The items in Category 1 have been summarized in Chapter II.C and need not be restated, but to these I will add assumptions and approximations from other categories, which will be useful in the development of a solution.

1. Category 2

Consideration of the curves in Fig. 6 suggests that electron temperature is independent of height above about 300 km. Figures 4 and 5 suggest that this condition is approximately true above 500 km. Consideration of Fig. 3 suggests that, at least above 500 km, ion temperature increases significantly with height by day, and increases with height very slowly or not at all by night. In addition, Fig. 6 suggests that electron temperature is higher at higher latitudes, at least by day, and that the latitudinal gradient of electron temperature is small. From these considerations we can formalize the following approximations, valid for heights greater than 500 km:

$$\partial T_e/\partial h \approx 0 \qquad \text{by day and night}$$

$$\partial T_i/\partial h \gg 0 \qquad \text{by day}$$

$$\partial T_i/\partial h \geq 0 \qquad \text{by night}$$

Latitudinal gradients of T_e (and probably T_i) are small, at least by day, and probably positive, at least at lower altitudes.

It is important to note that there is no direct evidence of the behavior of high-altitude, high-latitude electron and ion temperatures, nor is there detailed evidence of latitudinal variations of temperatures at any height. Also note, however, that the theoretical work of Hanson agrees with these results, particularly those of Fig. 3.

2. Category 3

A great deal of effort by a number of workers has gone into an attempt to determine whether or not a regular, large-scale flux of ionized particles is an important process in the topside ionosphere.

Quinn and Nisbet (1965), investigating the problem experimentally, have obtained an approximate value for a diffusion coefficient. Shimazaki (1959), for the special case of $\partial T/\partial h$ constant, considered the problem from a theoretical standpoint as part of the general problem of the continuity equation. Hanson and Patterson (1964) investigated the possibility that a downward-diffusion flux at night might be responsible for the maintenance of the nighttime F layer. On the assumption that such a downward flux at night must have as its source an equal and opposite (upward) flux by day, they conclude that the maximum possible upward flux by day is insufficient to provide the required downward flux at night.

From these and other similar efforts it has not been possible thus far to obtain an accurate determination of ionization flux. The results obtained by Quinn and Nisbet and also by Hanson and Patterson suggest an upper limit on the order of 10^8 particles/cm^2-sec.

The question of the importance of a nonzero flux in the topside ionosphere must be regarded as still open. With this in mind, I conducted the present study along two separate lines--zero flux ($W = 0$), and nonzero flux ($W \neq 0$)--using the following assumptions.

1. For nighttime midlatitude considerations for both models, the approximations of Category 2 suggest that $\partial(T_e + T_i)/\partial h$ is small. For convenience, then, in the nighttime, midlatitude, numerical solutions it is convenient to approximate temperatures by the first two terms of a power series--i.e., $T(h) = T_o(1+Ah)$.
2. For both models, the daytime problem is made analytically tractable by assuming that the gravitational field is independent of height.

Since my analysis is limited to heights between 500 and 800 km, such an approximation introduces only a small error into the results.

3. For the case of a nonzero flux, I use the assumptions that all particles are in thermal equilibrium ($T_e = T_i = T$), and that $\partial T/\partial h$ is constant. It should be pointed out that, from the assumption $q = L = 0$, made earlier, the nonzero flux is nondivergent (nW independent of height). This assumption is applied only to the consideration of the daytime problem.

B. PROCEDURE TO BE FOLLOWED

The problem, as defined earlier, is this: to determine the topside-ionosphere electron temperature, ion temperature, and the distribution of ion concentrations using as data, scale-height information obtained from the Alouette topside-sounder satellite.

Using arguments derived from a consideration of the physics of the ionosphere, I have justified certain reasonable assumptions. From consideration of the results of "direct" measurements of temperatures by other workers I have justified other assumptions. Finally, I have listed certain other assumptions that will be needed throughout this study, and have commented on the justification of each.

To analyze my data and draw more meaningful conclusions from them in an orderly manner, I follow the procedure outlined below.

1. Examine the program of observations obtained from the Alouette satellite by examining the experiment, the orbital parameters of the satellite, the spatial limitations of the data acquisition, and the resulting data. A brief outline of the method used to obtain scale-height data from the sounding echos is given in Appendix A, although the determination of scale height profiles is not of direct concern here, having been described in detail in other reports.
2. Develop a diffusive-equilibrium, three-constituent model ionosphere from which a definitive expression for scale height can be obtained in terms of electron temperature, ion temperature, and mean ionic mass.

3. Using some of the temperature results of other workers, make reasonable estimates of nighttime, midlatitude, ion distributions. Compare these results with those reported by Bowen et al.
4. Show, as a result of 3. that a definite transition level exists at which the ion constituency changes from predominantly ionized oxygen (O^+) to predominantly lighter ions (He^+, H^+). Study the latitudinal and temporal variations of this transition level.
5. For situations in which it can be reasonably assumed that the transition level lies well above the region of interest, perform a simplified analysis and interpret scale-height variations entirely in terms of temperature variations.
6. Consider the existence of a nonzero ionization flux for the daytime case and give an approximate solution.

V. THE EXPERIMENT AND THE EXPERIMENTAL OBSERVATIONS

The experimental source of electron scale-height data is the Alouette satellite topside sounder. To interpret the data properly, it is appropriate to review briefly the pertinent aspects of the experiment and the reduction of the data.

A. TOPSIDE-SOUNDER EXPERIMENT

The Canadian topside sounder, Alouette, was put into earth orbit on 29 September 1962 [C.D.R.T.E. (1962), Warren (1962)]. The information below is abstracted from the above references.

Frequency sweep	0.45 Mc to 11.5 Mc at a rate of 1 Mc/sec
Transmitter pulsewidth	100 μsec
Receiver noise figure	8 db
Pulse repetition frequency	67 cps
Frequency sweep period	18 sec

The essential orbital elements of the satellite, given below, were computed from Minitrack observations at the NASA Computation Center for the 29 September 1962 date.

Anomalistic period	105.4 min
Inclination	80.46 deg
Motion of the argument of perigee	-2.5666 deg/day
Motion of the right ascension of the ascending node	-.984 deg/day
Perigee	999 km
Apogee	1032 km
Velocity at perigee	7.35 km/sec
Velocity at apogee	7.33 km/sec

As shown in the above tables, the sounder sweeps from 0.45 to 11.5 Mc at a rate of 1 Mc/sec, and the sweep is repeated every 18 sec. The satellite thus moves on the order of 50 km during the time a single sounding is taking place, and successive soundings are displaced approximately 132 km, or somewhat less than 1 deg of latitude in the region of interest. Large-scale variations in the ionosphere resulting from geographic effects should therefore not be noticed during one sounding and should present only gradual changes between successive soundings.

In addition, the eccentricity of the orbit is so small that the approximation that the altitude of the satellite is constant at 1000 km leads to a maximum error in height of 32 km, with the mean error only about 14 km. In addition, the precession of the orbit is so small that soundings taken over a period of several weeks are quite self consistent in height, with negligible error between them.

Since 4 December 1962, signals from the Alouette have been monitored on a routine basis by the satellite receiving station at the Radioscience Laboratory of Stanford University. The approximate geographic area within which the satellite signals have been monitored is shown in Fig. 1.

B. OBTAINING SCALE-HEIGHT PROFILES FROM IONOGRAMS

Details of the acquisition of the telemetered data by the recording station are described in Thomas and Sader (1964). As described in that report, the telemetry signals received are recorded on magnetic tape and later transferred to 35-mm film, providing a photographic record of each sounding. The filmed records may then be considered as plots of the virtual depth of reflection below the satellite as a function of sounding frequency and are commonly known as ionograms.

The reduction of ionograms to electron-density--N(h)--profiles has been studied and practiced in the case of bottomside analysis for many years. The use of the same techniques for topside analysis is complicated somewhat by the fact that the sounder is immersed within the plasma. Nevertheless, the difficulties appear to be well understood and techniques are available for performing this operation on a routine basis. The method used for the reduction of these data is described in Thomas and Westover (1963), and Thomas et al (1964), and is outlined briefly in the Appendix.

The reduction was actually performed through a joint effort of the Space Sciences Division of Ames Research Center, and Stanford Research Institute. The format of each profile was that of a tabulation of values of electron density at depths of 0, 50, and 100 km, etc. below the satellite, down to the level of maximum electron density, below which no data were received. A corresponding tabulation of scale-height values (in kilometers) was easily obtained in accordance with the definition of Eq. (6) by using "first differences" of electron density--that is, at any height h_o,

$$\frac{dn_e}{dh} \approx \frac{n_e(h_o + 50) - n_e(h_o - 50)}{100} \tag{40}$$

and

$$\mathcal{H}(h_o) \approx \frac{n_e(h_o) \times 100}{n_e(h_o - 50) - n_e(h_o + 50)} \cdot \tag{41}$$

This method provided tabulated values of $\mathcal{H}(h)$ defined at 50-km intervals below the satellite. Since successive soundings took place less than 1-deg apart in latitude, closely spaced information was obtained on the variation of scale height both with height and with latitude.

C. THE EXPERIMENTAL OBSERVATIONS

As a reasonable compromise between reducing data scatter and maintaining sensitivity to latitudinal variations, these individual profiles have been averaged over 3-deg latitude intervals so that, for purposes of this analysis, a profile that is associated with a given latitude is actually the mean profile obtained by averaging all individual profiles obtained within 1.5 deg of the given latitude. Latitudinal plots of scale height thus have a data point every 3 deg and are insensitive to changes of a smaller scale than this. The advantage gained is a significant improvement in the scatter characteristics of the data.

The data to be considered are limited to the region between 50- and 85-deg latitude and between 500 and 800 km in height. The station at Stanford is a receiving station only; it has no command capabilities.

Since the sounder operates only on command, the data acquired at Stanford depend on the satellite's being simultaneously within the line of sight of Stanford and within the line of sight of stations containing a command capability. In addition, the sounder is not commanded especially for the benefit of the Stanford receiving station. The stations providing the most advantageous commands are College, Alaska, and Grand Forks, Minnesota. The geographic locations of these stations tend to concentrate most of the data acquisition to the higher latitudes--i.e., from 50-deg dip latitude to 85-deg dip latitude.

The height limits are set by other considerations. The lower limit is established as 500 km, to avoid the complicating effects of recombination at lower heights, thus allowing interpretation of results in terms of a very simple model. The upper limit is also set by practical problems. The virtual depth of signal penetration in the vicinity of the satellite increases very rapidly with a small increase in sounding frequency; as a result, the ionogram trace has a very steep gradient there, so steep that it becomes difficult to scale visually. Paul and Wright (1964) examined this problem and showed that the ionogram trace approaches an infinite gradient at the satellite, thus making the records difficult to interpret. The scale-height profiles I have analysed have also shown this effect, being quite consistent up to 800 or 850 km, and showing randomly erratic behavior above, thus determining an upper limit of 800 km for my research.

The data were acquired during the periods May through July 1963 and November 1963 through January 1964. In any three-month period the satellite's orbit precesses slightly less than 180 deg so that, in each of these two periods, a nearly complete diurnal variation of data was obtained.

In general, data acquired during the summer period were more plentiful and of higher quality than the winter data, especially data from nighttime passages. More passages were recorded in the summer period than in the winter, and the percentage of nighttime recordings was higher in the summer than in the winter. On many of the ionograms the plasma frequency at the vehicle could not be determined because of noise or other effects. Of the remaining ionograms, some were rejected because of errors in scaling (about 20 percent of the winter nighttime ionograms were rejected for this reason). The net result was that the accuracy of the winter nighttime analysis suffers to some extent from insufficient data.

The data for both seasons were studied for their dependence on different coordinate variations and have been plotted in Figs. 7 through 11. I shall point out certain outstanding features of each of these figures in turn which will be studied and interpreted in various ways throughout the report.

Figure 7 is a plot of scale height as a function of height at a series of latitudes for a single satellite passage, which took place 1 June 1963,

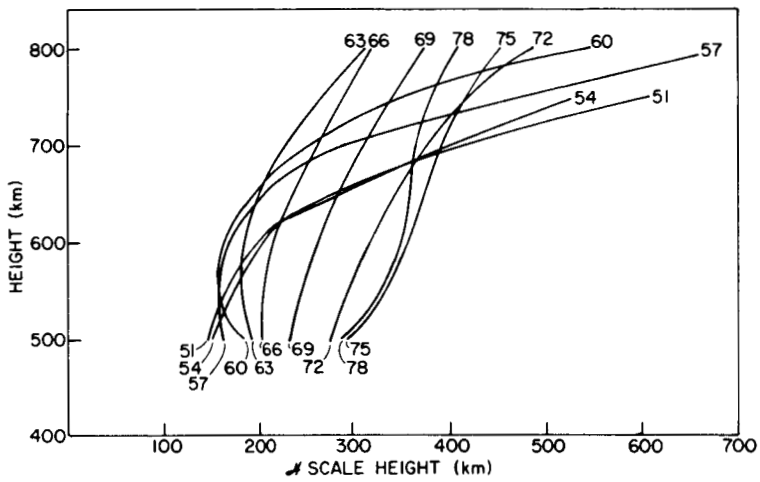

33207

FIG. 7. EXPERIMENTAL RESULTS FROM TYPICAL NIGHTTIME PASSAGE, SHOWING SCALE-HEIGHT PROFILES AT A SERIES OF DIP LATITUDES AND ILLUSTRATING THE VARIATION OF THE PROFILES WITH LATITUDE. Data obtained from Passage No. 3346, 0200 - 0330 LMT, 1 June 1963.

between 0250 and 0330 Local Mean Time (LMT); the data, however, are typical for periods from 2300 to 0400 LMT and for both summer and winter records. As noted before, each curve, or $\mathcal{H}$ profile, is associated with a certain latitude and is actually an average of two or three individual profiles grouped around that latitude. There are several interesting features of this group of profiles. Notice that, at the lower latitudes, there is a definite hook or elbow to the profiles, a feature that is absent at the higher latitudes. Below this hook, $\mathcal{H}$ increases very slowly with height and above this hook, $\mathcal{H}$ increases rapidly with height. At the lower latitudes the curves appear to be displaced upward with increasing latitude until, by latitude 66 deg, the hook has risen higher than 800 km and is no longer evident. Thereafter, the curves move to the right--i.e., increasing $\mathcal{H}$ with increasing latitude. A slight reversal of this last trend seems to take place above 75 deg latitude.

Figure 8 is a great contrast to Fig. 7. It represents data from a passage occurring 10 June 1963, from 1130 to 1250 LMT. It is typical, however, of daytime (0800 - 1700 LMT) data for both summer and winter. Only two profiles are plotted because all data occurred within the narrow region indicated by the dotted lines. The general character of these daytime profiles was that there was only very slight latitude dependence and that, at all latitudes, scale height varied almost linearly with height.

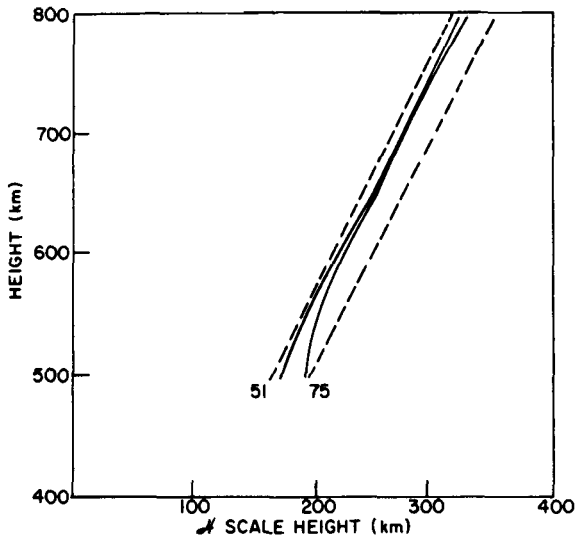

33208

FIG. 8. EXPERIMENTAL RESULTS FROM TYPICAL DAYTIME PASSAGE, SHOWING SCALE-HEIGHT PROFILES AT TWO WIDELY SEPARATED DIP LATITUDES AND ILLUSTRATING THE CONSISTENCY OF THE DAYTIME RESULTS. All the data for the entire passage, if plotted, would lie between the dotted lines. Data obtained from Passage No. 3473, 1140 - 1250 LMT, 10 June 1963.

Figure 9 emphasizes the difference in diurnal variation at two different latitudes for summer and winter respectively. Each curve is obtained by averaging the data from 15 or more passages. The daytime curves represent the average of all data recorded from 0800 to 1700 LMT. The nighttime curves represent the average of all data recorded from 2300 to 0400 LMT. It can be seen from the figure that diurnal variation is strongly dependent on latitude. This dependence will be quantitatively explored in following sections.

Figure 10 illustrates the variations of daytime scale heights with latitude for summer and winter respectively. Each of these plots was

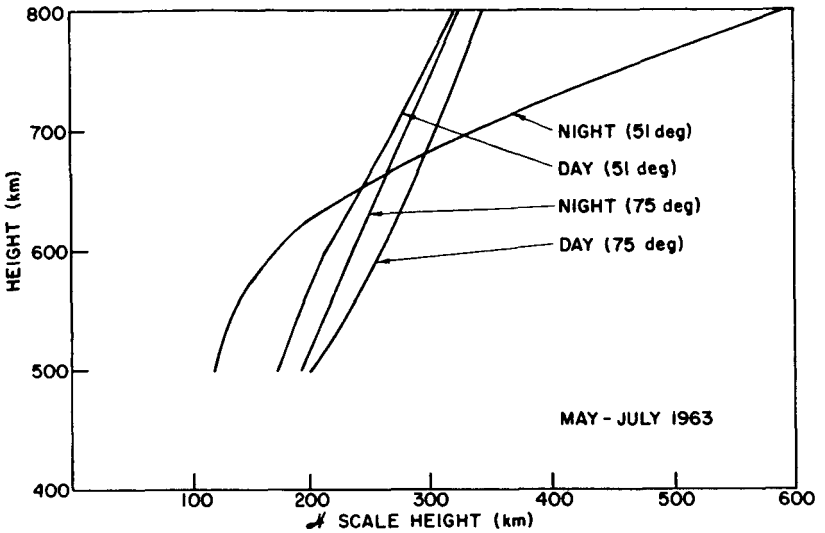

33209

a. Summer, May - July 1963

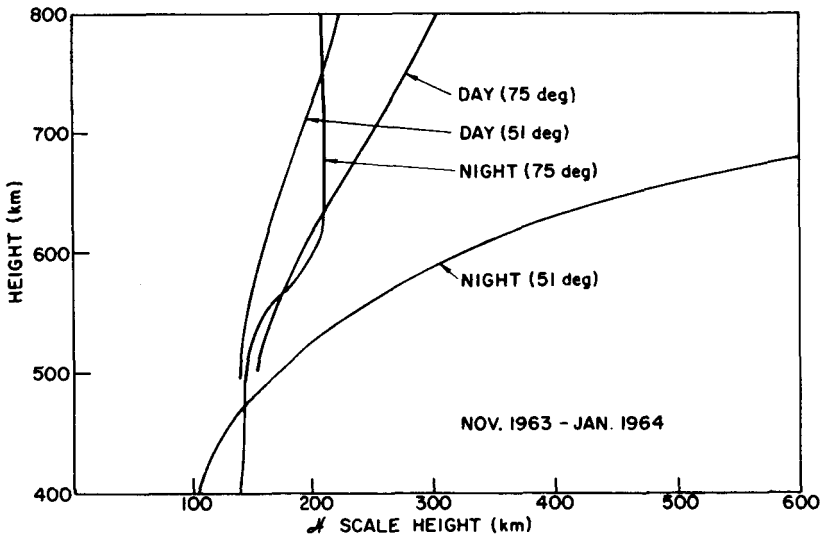

33210

b. Winter, November 1963 - January 1964

FIG. 9. COMPARISON OF DAYTIME AND NIGHTTIME SCALE-HEIGHT PROFILES AT TWO WIDELY SPACED DIP LATITUDES, SHOWING THE CONTRAST AT THE LOWER LATITUDES AND THE SIMILARITY AT THE HIGH LATITUDES. Each curve represents the average of data from at least 15 passages occuring during the period covered.

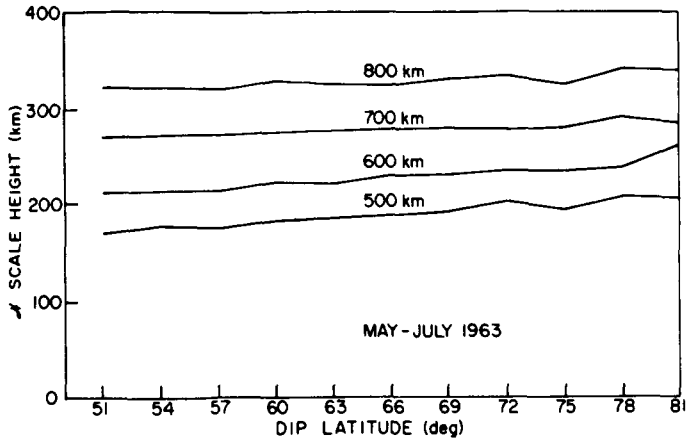

33211

a. Summer, May - July 1963

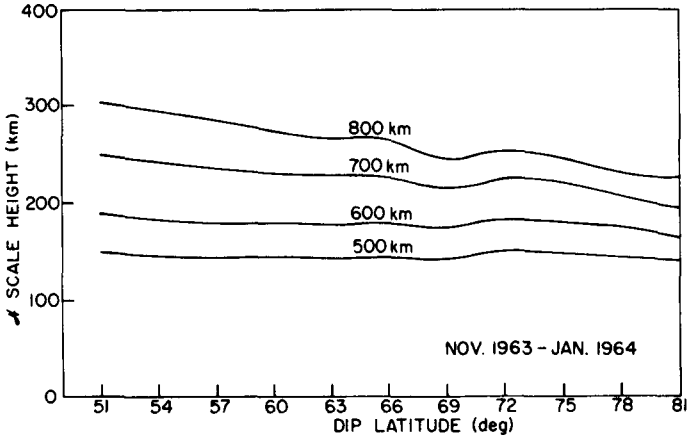

33212

b. Winter, November 1963 - January 1964

FIG. 10. DAYTIME SCALE HEIGHT AS A FUNCTION OF DIP LATITUDE AT FOUR ALTITUDES. Each curve represents the average of data obtained from at least 15 passages occurring between 0800 and 1700 LMT.

obtained from the average of a series (15 to 20) of passages occurring between 0800 and 1700 LMT. Note that the summer profiles increase slightly with latitude at all altitudes, while the winter profiles are nearly independent of latitude at 500 km and decrease with latitude at the higher altitudes.

Figure 11 illustrates the variations of nighttime scale heights with latitude for summer and winter respectively. These plots were obtained by averaging the data from a series of passages occurring between 2300 and 0400 LMT. The trend shown in Fig. 7 is apparent here also. The scale height at 500 km increases smoothly with latitude, while the scale heights at higher altitudes decrease sharply with latitude at first and show a much milder variation at higher latitudes. The dotted line in each plot represents the latitude dependence of the O^+-He^+, H^+ transition level. The derivation and interpretation of the transition level result from my theoretical model and are discussed in detail in a later section.

Figures 7 through 11 represent all the "raw" data from the Alouette sounder with which this report is concerned. In the following sections the interpretation of these data are considered in terms of ion number density and temperature distributions.

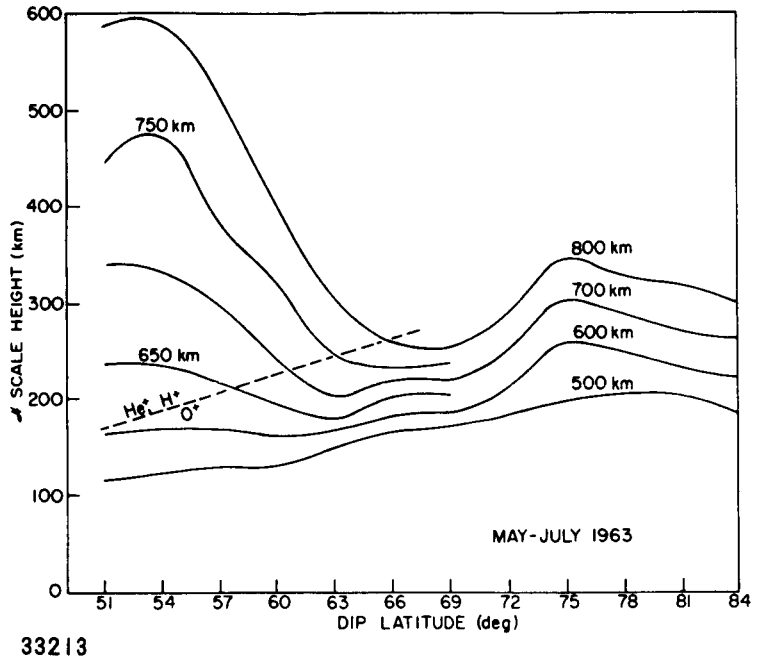

a. Summer, May - July 1963

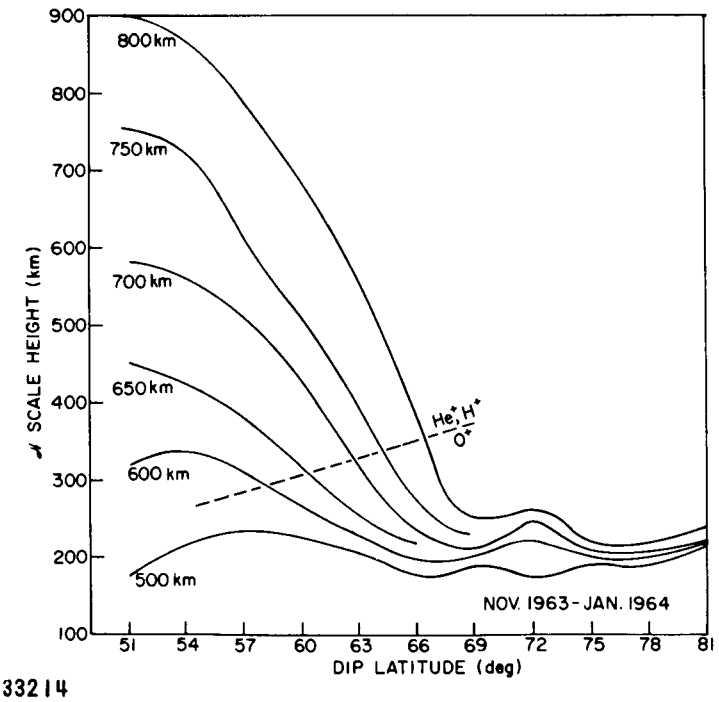

b. Winter, November 1963 - January 1964.

FIG. 11. NIGHTTIME SCALE HEIGHT AS A FUNCTION OF DIP LATITUDE AT A SERIES OF ALTITUDES. Each curve represents the average of data obtained from at least 15 passages occurring between 2300 and 0400 LMT. The dotted line represents the transition level (O^+-He^+, H^+).

VI. THEORY OF STATIC DIFFUSIVE EQUILIBRIUM

A. DEVELOPMENT OF A MODEL

Consider the static case of theoretical distribution of ions and electrons (in which there is no flux of particles present) in the region bounded by heights of 500 km and 800 km, and dip latitudes of 50° and 85° North. The case of a nonzero flux is treated in Chapter VIII.

The following simplifying assumptions are appropriate, all of which were considered in Section IV.A.

1. The ionosphere consists entirely of neutral particles and a statistically neutral mixture of electrons and singly charged ions of oxygen (O^+), helium (He^+), and hydrogen (H^+).
2. The medium is in a state of diffusive equilibrium; thus diffusion is the dominant process controling the distribution of electrons and ions, and the effects of production, loss, and time derivatives of all quantities can be neglected.
3. The ionosphere is horizontally stratified--i.e., horizontal gradients of all quantities are much smaller than vertical gradients.
4. There is no net transport velocity associated with any species.
5. In any small region of space, all ions are in thermal equilibrium among themselves.

For conditions such as these, in which there is no production or loss, the equilibrium distribution of any species can be obtained by forming a balance of all forces present. For this case the appropriate force equation for each species is obtained by balancing the pressure gradient against all other forces, as

$$\nabla p = ne\bar{E} + \bar{F} \tag{42}$$

where

$$p = nkT \ . \tag{43}$$

Here p is the partial pressure of any species of particle, T is particle temperature, $\bar{E}$ is any electric field present, and $\bar{F}$ accounts for all noncoulomb forces present. In the case of a rotating earth, $\bar{F}$ is

the sum of gravitational and centripetal forces--i.e.,

$$\bar{F} = -nmg\ \bar{a}_r + nm\omega^2 R \cos\varphi\ \bar{a}_\gamma \tag{44}$$

where $\bar{a}_r$ is a unit vector in the radial direction, $\bar{a}_\gamma$ is a unit vector perpendicular to the axis of rotation, R is the radial distance from the earth's center, and φ is the angle between $\bar{a}_r$ and the earth's equatorial plane.

The radial component of $\bar{F}$ is

$$\bar{F}\cdot\bar{a}_\varphi = nm\omega^2 R \cos\varphi \sin\varphi\ . \tag{46}$$

The centripetal contribution to $\bar{F}$ can be neglected. The maximum centripetal contribution occurs at the maximum height (800 km) and in the equatorial plane. Using an earth radius of 6380 km, compare the relative magnitudes of the terms in Eq. (45). In mks units,

$$\frac{\omega^2 R}{g} \approx 4 \times 10^{-3}\ . \tag{47}$$

On this basis, the centripetal contribution may be neglected. Equation (43) now becomes:

$$\frac{dp}{dh} = ne\bar{E} - nmg \tag{48}$$

where h is a coordinate in the radial direction. Note that if charge e is zero, Eq. (48) reduces to the statical equation of a neutral atmosphere,

$$\frac{dp}{dh} + nmg = 0\ . \tag{49}$$

Combining Eqs. (43) and (48) gives

$$\frac{d}{dh}\left(n_e k T_e\right) = -\,n_e m_e g - n_e |e| E \tag{50}$$

for electrons, and

$$\frac{d}{dh}\left(n_i kT_i\right) = - n_i m_i g + n_i |e| E \tag{51}$$

for each ion species.

Differentiation of Eqs. (50) and (51) results in

$$kT_e \frac{dn_e}{dh} + kn_e \frac{dT_e}{dh} = - n_e m_e g - n_e |e| E \tag{52}$$

$$kT_i \frac{dn_i}{dh} + kn_i \frac{dT_i}{dh} = - n_i m_i g + n_i |e| E \ . \tag{53}$$

From assumption (1),

$$n_e = \sum_i n_i \ . \tag{54}$$

Differentiating (54) gives

$$\frac{dn_e}{dh} = \frac{d}{dh}\sum_i n_i = \sum_i \frac{dn_i}{dh} \ . \tag{55}$$

Dividing Eq. (53) by kT_i and summing over all ion species, results in

$$\sum_i \frac{dn_i}{dh} = -\sum_i \frac{n_i}{T_i}\frac{dT_i}{dh} - \sum_i \frac{n_i m_i g}{kT_i} + (|e| E)\sum_i \frac{n_i}{kT_i} \ . \tag{56}$$

Combining Eqs. (52), (55), and (56), and noting by Assumption 5 that all ions have the same temperature lead to the solution for $|e| E$ as

$$|e| E = \left[\left(\frac{1}{T_i}\right)\left(\sum_i \frac{n_i m_i g}{k} + n_e \frac{dT_i}{dh}\right) - \left(\frac{1}{T_e}\right)\left(\frac{n_e m_e}{k} + n_e \frac{dT_e}{dh}\right)\right]\left[n_e\left(\frac{1}{kT_i} + \frac{1}{kT_e}\right)\right]^{-1} \tag{57}$$

It is a reasonable assumption that T_e and T_i are of the same order of magnitude. Then, since $m_e \ll m_i$, the term containing m_e is negligible. Designating space derivatives by primes, multiplying through by kT_e, and introducing the symbol $\tau = T_e/T_i$, lead to a more useful form of Eq. (57):

$$|e|E = \left[\tau\left(\sum_i n_i m_i g + n_e kT_i'\right) - n_e kT_e'\right]\left[n_e(1+\tau)\right]^{-1} . \qquad (58)$$

This quantity has the dimensions of force, so for convenience I define a new quantity by the relation

$$|e|E = \frac{Mg}{2} . \qquad (59)$$

Deferring the solution of Eq. (58) for the moment, combine Eq. (59) with Eqs. (50) and (51), to obtain

$$\frac{d}{dh}(n_e kT_e) = - n_e\left[m_e + (M/2)\right]g \qquad (60)$$

and

$$\frac{d}{dh}(n_i kT_i) = - n_i\left[m_i - (M/2)\right]g . \qquad (61)$$

It is subsequently shown that, in all cases, $M \gg m_e$ so that Eq. (60) reduces to

$$\frac{d}{dh}(n_e kT_e) = - \frac{n_e Mg}{2} . \qquad (62)$$

An expression for scale height can be derived from Eq. (62). Then

$$d(n_e kT_e) = - \frac{n_e Mg}{2} dh = - \frac{n_e kT_e Mg}{2kT_e} dh \qquad (63)$$

and

$$\frac{d(n_e kT_e)}{n_e kT_e} = \frac{Mg}{2kT_e}\, dh \ . \tag{64}$$

Integrating between a reference level $h = 0$ and a level $h = z$ leads to

$$\frac{n_e(z)\ T_e(z)}{n_{eo}\ T_{eo}} = \exp\left[- \int_o^z \frac{Mg}{2kT_e}\, dh \right] \tag{65}$$

and

$$n_e(z) = \frac{n_{eo}\ T_{eo}}{T_e(z)} \exp\left[- \int_o^z \frac{Mg}{2kT_e}\, dh \right] . \tag{66}$$

Differentiating (66) gives

$$\frac{dn_e}{dz} = \left[- \frac{T_e'}{T_e} - \frac{Mg}{2kT_e} \right] \left[\frac{n_{eo}\ T_{eo}}{T_e} \exp\left(- \int_o^z \frac{Mg}{2kT_e}\, dh \right) \right] \tag{67}$$

For brevity, I have deleted the z notation, but it is understood that all quantities under the integral are functions of the height variable h and all other quantities are functions of the height variable z.

Dividing (67) by (66) results in

$$\frac{1}{n_e} \frac{dn_e}{dz} = - \frac{T_e'}{T_e} - \frac{Mg}{2kT_e} \ . \tag{68}$$

From the definition of scale height, note

$$\mathcal{H} = \left[\frac{T_e'}{T_e} + \frac{Mg}{2kT_e} \right]^{-1} \tag{69}$$

where M is given by:

$$M = \frac{2}{g}\left\{\left[\tau\left(\sum_i n_i m_i g + n_e k T_i'\right) - n_e k T_e'\right]\left[n_e(1+\tau)\right]^{-1}\right\} . \qquad (70)$$

Introducing the definition for mean ionic mass,

$$\langle m_i \rangle = \left(\sum_i n_i m_i\right)\left(\sum_i n_i\right)^{-1} \qquad (71)$$

permits simplifying Eq. (70) to

$$M = \frac{2}{g}\left[\frac{\tau\left(\langle m_i \rangle g + k T_i'\right) - k T_e'}{1 + \tau}\right] . \qquad (72)$$

M cannot be found directly from Eq. (72) since $\langle m_i \rangle$ is an unknown function of height. Later on, it will be possible to make certain assumptions about $\langle m_i \rangle$, but for the present, other means to determine M must be used.

The method of development of Eqs. (63) through (66) yields solutions for ion number densities. From Eq. (61),

$$d\left(n_i k T_i\right) = -\frac{n_i\left(2m_i - M\right)g}{2}\, dh = -\frac{n_i k T_i\left(2m_i - M\right)g}{2kT_i}\, dh \qquad (73)$$

and

$$\frac{d\left(n_i k T_i\right)}{n_i k T_i} = \frac{\left(M - 2m_i\right)g}{2kT_i}\, dh . \qquad (74)$$

Integrating between $h = 0$ and $h = z$, yields

$$\frac{n_i\, T_i}{n_{io}\, T_{io}} = \exp\left[\int_o^z \frac{\left(M - 2m_i\right)g}{2kT_i}\, dh\right] \qquad (75)$$

and

$$n_i = \frac{n_{io}\, T_{io}}{T_i} \exp\left[\int_o^z \frac{\left(M-2m_i\right)g}{2kT_i}\, dh\right] , \tag{76}$$

where, as before, the functional notation z has been omitted for brevity. Summing n_i over all ions and referring to Eqs. (54) and (66) leads to

$$\frac{n_{eo}\, T_{eo}}{T_e} \exp\left[-\int_o^z \frac{Mg}{2kT_e}\, dh\right] = \frac{T_{io}}{T_i}\sum_i n_{io} \exp\left[\int_o^z \frac{\left(M-2m_i\right)g}{2kT_i}\, dh\right] . \tag{77}$$

For a three-constituent ionosphere, the solution of Eq. (77) requires the specification of the two temperature functions T_e and T_i, and three of the four densities at some height, say, $z = 0$.

By using Eq. (76), I can express $\langle m_i \rangle$ in terms of these variables. Then,

$$\langle m_i \rangle = \frac{\sum_i n_i m_i}{\sum_i n_i} = \frac{\sum_i n_{io} m_i \exp\left[\int_o^z \frac{\left(M-2m_i\right)g}{2kT_i}\, dh\right]}{\sum_i n_{io} \exp\left[\int_o^z \frac{\left(M-2m_i\right)g}{2kT_i}\, dh\right]} \tag{78}$$

which becomes, on removing the common factor,

$$\langle m_i \rangle = \left\{\sum_i n_{io} m_i \exp\left[-\int_o^z \frac{m_i g}{kT_i}\, dh\right]\right\}\left\{\sum_i n_{io} \exp\left[-\int_o^z \frac{m_i g}{kT_i}\, dh\right]\right\}^{-1} . \tag{79}$$

Similarly, the fractional proportion of any single ion constituent may be expressed by

$$P_j = \frac{n_j}{\sum_i n_i} = \left\{n_{jo} \exp\left[-\int_o^z \frac{m_j g}{kT_i}\, dh\right]\right\}\left\{\sum_i n_{io} \exp\left[-\int_o^z \frac{m_i g}{kT_i}\, dh\right]\right\}^{-1} , \tag{80}$$

where $T_i = T_j$. It is important to notice that $\langle m_i \rangle$ and P_j are independent of electron temperature. This means, of course, that at any arbitrary height, the relative concentration of any particular ion species is independent of electron temperature.

The model derived can now be described as follows:

1. There are four number densities and two temperature functions that vary with height. By the assumption of charge neutrality, only three of the densities need be specified independently. The model then requires that electron temperature and ion temperature be specified at all heights and that three number densities be specified at one arbitrary height.
2. Following 1., Eq. (77) can be solved numerically for $M(z)$ and Eq. (80) can be solved numerically for $P_i(z)$, noting again that $P_i(z)$ does not depend on T_e.
3. Following 2., Eqs. (66), (69), and (76) can be solved numerically for $n_e(z)$, $\mathcal{H}(z)$, and $n_i(z)$ respectively.
4. Following 3., $\mathcal{H}(z)$ can be compared with experimental scale-height profiles.

B. NUMERICAL RESULTS

Numerical solutions were obtained by writing a computer program to solve Eqs. (66), (69), (76), (77), and (79), and then, for any set of assumed values for the required number densities and temperature functions, compare Eq. (69) with an experimental scale height profile. The night (51 deg) curve of Fig. 9a was used first, since it represented conditions reasonably close to those of the Ariel data mentioned earlier. In examining this experimental profile, it became obvious that, if electron and ion temperatures were reasonably independent of altitude, then the "bend" or "hook" in the profile at a height of about 600 km must represent a transition from one ion species to another. Furthermore, comparison of reasonable values of temperature with observed values of scale height through Eq. (69) indicated that the transition must be from O^+ to a lighter ion.

The determination of numerical solutions beyond this point involved trial and error, families of solutions, and empirical curve-fitting. It was found by trial and error that the specification of 50 percent O^+ ions at 600 km appeared to provide a better "fit" with the experimental profile

than did 50 percent O^+ at either 550 or 650 km, and this was true over a wide variety of assumptions about the other parameters. The procedure then went as follows:

1. The reference height $z = 0$ was placed at 600 km and the relative concentration of O^+ at that level was fixed at 50 percent.
2. In conformance with the assumption that nighttime midlatitude temperature gradients are small, electron and ion temperature functions were limited to the first two terms of a power series--i.e.,

$$T_e(z) = T_{eo}(1 + A_e z) \tag{81}$$

$$T_i(z) = T_{io}(1 + A_i z) \quad . \tag{82}$$

3. Families of solutions were obtained for the following general categories of suppositions:

a. H^+ was assumed completely absent; various combinations of electron and ion temperatures were used, such as $T_e(z) = T_i(z)$, $T_e(z) =$ constant, or $T_i(z) =$ constant.

b. He^+ was assumed completely absent; various combinations of electron and ion temperatures were used, such as $T_e(z) = T_i(z)$, $T_e(z) =$ constant, or $T_i(z) =$ constant.

c. Electron and ion temperatures were assumed independent of height and resulting percentages of He^+ and H^+ were determined for various values of T_e/T_i.

Category a was used to provide a close approximation to the relative-number-density results of Bowen et al from the Ariel satellite. Category b was used to provide a constrast to Category a, in order to determine the sensitivity of my model to variations in percentage concentration. Category c was used to provide reasonable agreement with the electron and ion temperature results of Brace et al and Evans.

Some of the conclusions resulting from this analysis are shown in Tables 1 and 2, in which, for categories a, b, and c, I have illustrated the solutions for the conditions $T_e(z) = T_i(z)$, these solutions being representative of all the solutions obtained. Table 1 illustrates the

TABLE 1. MODEL PARAMETERS

Category	T_{eo} (°K)	T_{io} (°K)	∇T_e (°K/km)	∇T_i (°K/km)	P_{20} (%)	P_{30} (%)
a.	655	655	-1.05	-1.05	50	0
b.	880	880	1.06	1.06	0	50
c.	785	785	0	0	32	18

TABLE 2. EXPERIMENTAL VS THEORETICAL VALUES OF SCALE HEIGHT

Height (km)	Values of Scale Height $\mathcal{H}$			
	Experimental	Category		
		a	b	c
500	118	125	98	113
550	133	136	122	131
600	166	169	168	169
650	236	238	247	237
700	340	346	355	339
750	448	452	474	463
800	587	498	581	584

parameters that provided the best empirical fit between the theoretical $\mathcal{H}(z)$ and the experimental scale-height profile. Table 2 illustrates the degree of fit that was actually obtained in each case by comparing, at 50-km intervals of height, the experimental and the theoretical values of scale height. The experimental numbers were taken directly from the night (51 deg) profile of Fig. 9a.

It can be seen from Table 1 that Category a requires rather low temperatures and a negative temperature gradient. Category b requires somewhat higher temperatures and a positive temperature gradient. Category c requires comparable percentages of O^+, He^+, and H^+ at 600 km. The results of Table 2 indicate that Category c is capable of providing the best fit to the entire experimental profile.

Figures 12, 13, and 14 illustrate the ion percentage concentrations corresponding to Categories a, b, and c respectively. Consideration of all three figures illustrates that the percentages of minor ions changes rapidly with height. Figure 14 illustrates that, if there is appreciabe H^+ present at 600 km, He^+ can be a dominant ion at most over only a narrow height interval.

For comparison purposes I have illustrated the distribution of percentage concentrations for the Ariel results of Eqs. (37), (38), and (39), and the assumed temperatures of Category c--i.e., $T_e = T_i = 785\ ^\circ K$. It can be seen that the Ariel results suggest that the percentage of H^+ is negligible throughout the height range (500 to 800 km).

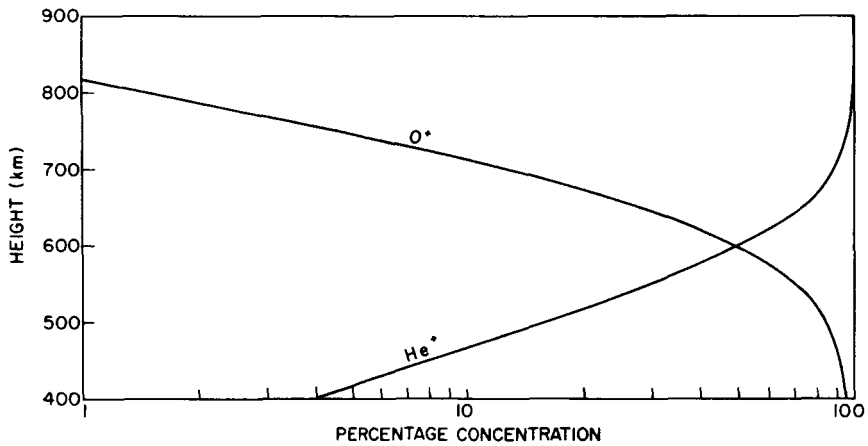

33220

FIG. 12. RELATIVE CONCENTRATIONS OF O^+ AND He^+ AS FUNCTIONS OF HEIGHT CORRESPONDING TO THE CONDITIONS:

H^+ is absent

Concentration of O^+ is 50 percent at 600 km

$T_e = T_i = 665\ ^\circ K$ at 600 km

$\nabla T = -1.05\ ^\circ K/km$.

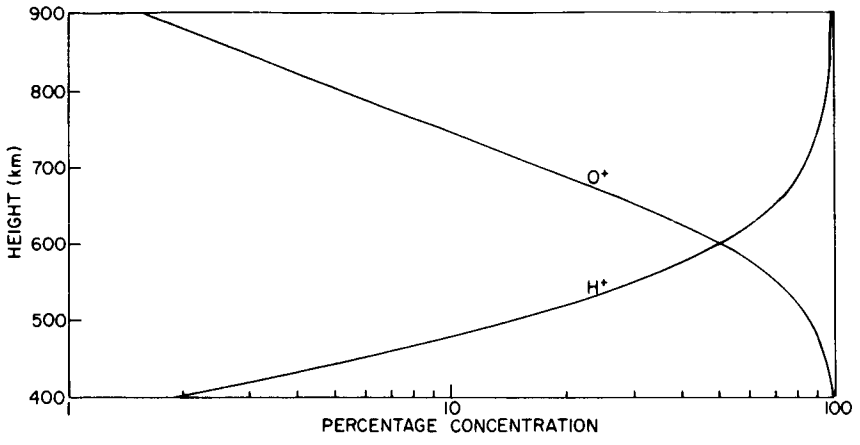

33221

FIG. 13. RELATIVE CONCENTRATIONS OF O^+ AND H^+ AS FUNCTIONS OF HEIGHT CORRESPONDING TO THE CONDITIONS:

He^+ is absent

Concentration of O^+ is 50 percent at 600 km

$T_e = T_i = 800\ ^\circ K$ at 600 km

$\nabla T = 1.06\ ^\circ K/km$.

From the observations just made, I draw the following conclusions about my model and about the appropriate region of the ionosphere:

1. Although the deflection of the experimental scale-height profile in the vicinity of 600 km indicates the existence of a transition from O^+ to lighter ions in this region, the arbitrary way in which the reference-level boundary--$P(O^+)$ = 50 percent at 600 km--was chosen suggests that a scale-height analysis will not lead to a determination of transition level closer than about ±25 km, unless some of the parameters (concentration vs height, temperature vs height) are known independently.

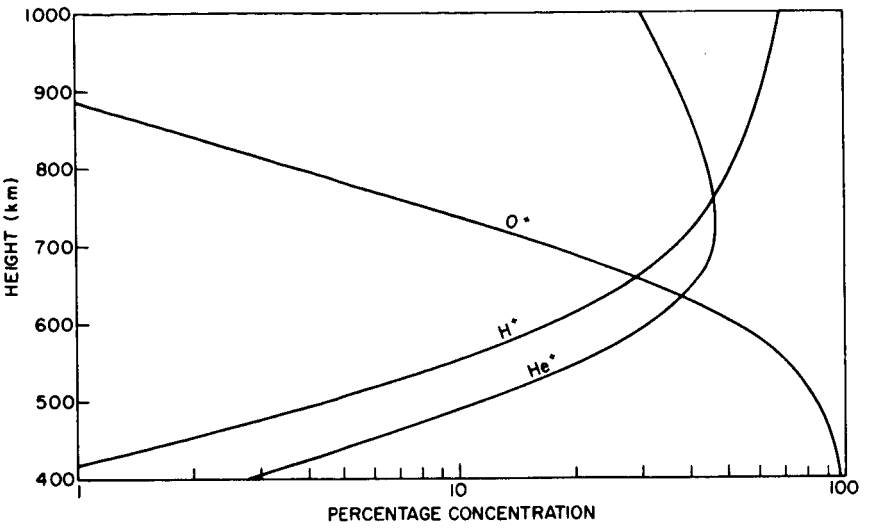

33222

FIG. 14. RELATIVE CONCENTRATIONS OF O^+, He^+, AND H^+ AS FUNCTIONS OF HEIGHT FOR AN ISOTHERMAL IONOSPHERE UNDER THE FOLLOWING CONDITIONS:

$T_e = T_i = 785\ ^\circ K$

Concentrations at 600 km are:

O^+ = 50 percent

He^+ = 32 percent

H^+ = 18 percent.

2. In the vicinity of the transition level, defined here by the condition $P(O^+) = 50$ percent, variations in scale height are very rapid and are controlled mainly by variations in the relative concentrations of the ions.
3. At distances as little as 150 km below the transition level, the relative concentrations of the light ions are negligible, and O^+ completely dominates.
4. If H^+ is in negligible concentration at the reference level, then negative temperature gradients are required to provide a reasonable

fit with measured data. The difficulty of obtaining a good fit in this case suggests that H^+ is not negligible at the reference level.

5. If He^+ is in negligible concentration at the reference level, then positive temperature gradients are required to provide a reasonable fit. Furthermore, if He^+ is negligible at the reference level, then it is negligible everywhere, while negligible H^+ at the reference level does not preclude a possible He^+-H^+ transition at a higher altitude.
6. An atmosphere in which temperatures are independent of height requires comparable concentrations of He^+ and H^+ at the reference level, with the result that H^+ becomes the dominant constituent a very short distance above the reference level.

The Ariel results, as shown in Fig. 15, suggest a rather wide range of height in which He^+ is the dominant ion. Conversely, the experimental scale-height profiles from the Alouette suggest that such a condition is not likely on the basis that: 1) it is difficult to obtain a good fit between experimental and theoretical results, 2) low temperatures and negative temperature gradients are required, both in conflict with

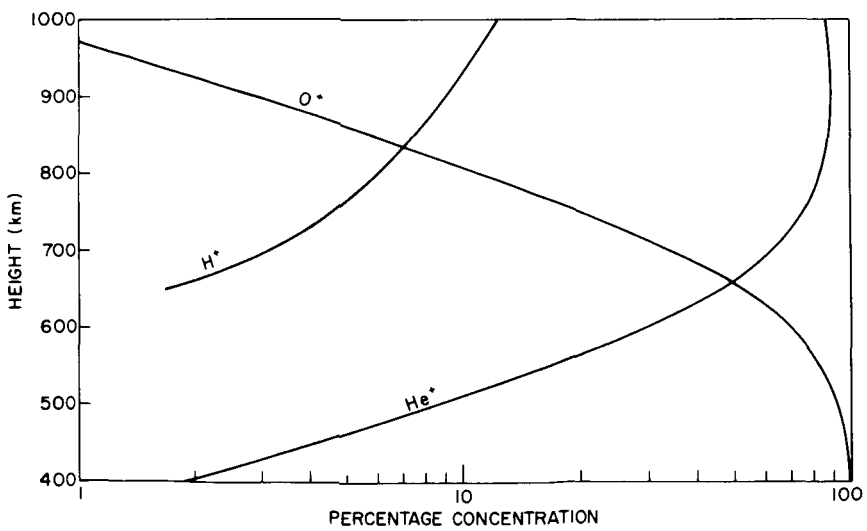

33224

FIG. 15. RELATIVE CONCENTRATIONS OF O^+, He^+, AND H^+ AS FUNCTIONS OF HEIGHT CORRESPONDING TO THE NIGHTTIME ARIEL TRANSITION LEVELS OF FIG. 2.

results such as those of Brace et al and Evans. Because there is some arbitrariness in my own results, I cannot specify exactly the extent of the disagreement, but it can be said that the Alouette results suggest substantially less He^+ in the topside ionosphere than do the results of the Ariel satellite. On the other hand, the two experiments agree quite well on the location of a transition level at about 600-km height.

VII. INTERPRETATION OF RESULTS

A. VARIATIONS OF THE TRANSITION LEVEL

The deflection of an experimental scale-height profile has been shown to indicate the existence of a transition from O^+ to He^+ and H^+ ions. The height at which this transition takes place can be determined to within an accuracy of, perhaps, ±25 km. It is now convenient to attempt to describe this transition level in a different manner than previously used.

Since transition is defined by the condition $P(O^+) = 50$ percent, then at the transition level for any arbitrary concentrations of He^+ and H^+, $\langle m_i \rangle$ must lie between 8.5 and 10 atomic mass units (amu). If temperature gradients are not too large it can be assumed that transition corresponds approximately to the condition:

$$\mathcal{H}_T \approx 1.6\, \mathcal{H}_{min}$$

where $\mathcal{H}_{min}$ is the minimum value of scale height and $\mathcal{H}_T$ is the value of the scale height at the transition level. When this description was applied to each scale height profile for <u>each</u> satellite passage, and the resulting transition height for each profile was plotted against the latitude at which it occurred,,it was seen that in all cases the resulting plot showed a monotonic increase with latitude. Figure 16 shows the results of drawing a smooth curve through values of transition level which were obtained at 3-deg-latitude intervals by averaging the results of a series of summer passages and a series of winter passages. These curves have also been plotted as dashed lines in Fig. 11. The striking variations of scale height with latitude between 54 °N and 69 °N may now be interpreted as resulting from an increase in the relative concentration of O^+ with latitude.

Two other important conclusions can be drawn from the curves in Fig. 16. First, as pointed out earlier, the relative ion concentration is independent of electron temperature. The curves suggest, therefore, that ion temperature increases with increasing latitude. Second, at depths as

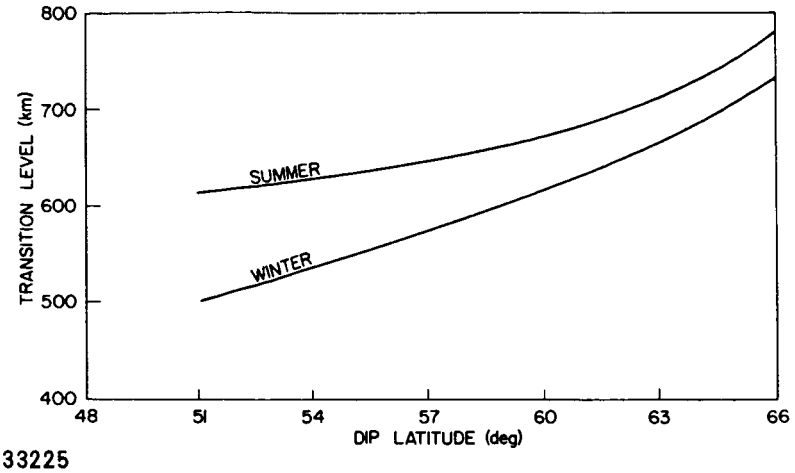

FIG. 16. NIGHTTIME TRANSITION LEVEL AS A FUNCTION OF LATITUDE FOR SUMMER (MAY - JULY 1963) AND WINTER (NOVEMBER 1963 - JANUARY 1964). Transition level is defined as the height at which the relative concentration of O^+ is 50 percent. Each curve is obtained from the average data from at least 15 passage occurring between 2300 and 0400 LMT.

small as 150 km below the transition level, O^+ concentration completely dominates, so that, at higher latitudes, variations in scale height must be due only to temperature effects.

Using the same method we can study the variation of transition level with time. Figure 17 shows a plot of transition level as a function of time for all profiles obtained at 51 ± 1.5 deg dip latitude. Considering that the Ariel results employed an idealized sinusoidal diurnal variation of temperature, a comparison of Fig. 17 with Fig. 2 indicates good agreement with the midlatitude results of Ariel.

Figure 17 suggests that the transition level rises rather sharply at dawn, descends somewhat more slowly at sunset, and either remains constant or descends very gradually through most of the night. One should be cautious about attempting to draw quantitative conclusions from the curve, since the assumption $\partial n/\partial t = 0$ may not be valid, but the evidence that the transition level is higher by day than by night is quite strong. If the daytime transition level is assumed at least as high as 950 km, then the approximation can be made that the ion composition in the region below 800 km is only O^+, and changes in daytime scale height can be interpreted entirely in terms of electron temperature and ion temperature.

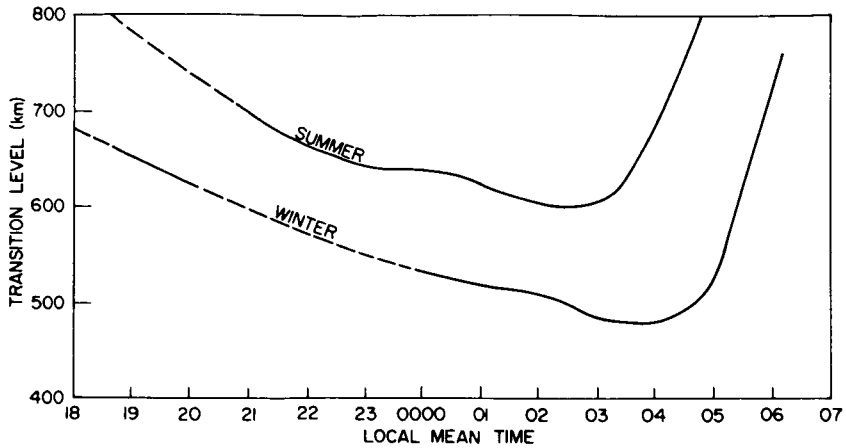

33226

FIG. 17. TRANSITION LEVEL AT 51-DEG DIP LATITUDE AS A FUNCTION OF TIME FOR SUMMER (MAY - JULY 1963) AND WINTER (NOVEMBER 1963 - JANUARY 1964). Transition level is defined as the height at which the relative concentration of O^+ is 50 percent. The dotted portions of the curves represent incomplete data.

B. INTERPRETATION OF DAYTIME SCALE HEIGHTS

Both summer and winter daytime midlatitude scale heights demonstrate the same behavior with respect to altitude. In both cases, scale heights increase nearly linearly from 500 to 800 km. I will now interpret these observations in terms of height variations in electron and ion temperatures, in the following way.

Scale height can be expressed directly in terms of ion and electron temperatures and mean ionic mass by combining Eqs. (69) and (72); thus,

$$\mathcal{H} = \left[\frac{\tau\left(T_e' + T_i' + \langle m_i \rangle\, g/k\right)}{(1+\tau)\, T_e}\right]^{-1} \tag{84}$$

which reduces to

$$\mathcal{H} = \frac{T_e + T_i}{T_e' + T_i' + \langle m_i \rangle\, g/k} \,. \tag{85}$$

For the special case $T_e' = T_i' = 0$, this simplifies to

$$\mathcal{H} = \frac{k\left(T_e + T_i\right)}{\langle m_i \rangle g} \quad . \tag{86}$$

It should be emphasized that Eq. (86), which is commonly used as a definitive expression for scale height, is not valid in the presence of temperature gradients. In such a case Eq. (85) is the appropriate expression.

To relate temperatures and temperature gradients to gradients in scale height, it is assumed that

$$\langle m_i \rangle \approx m(O^+) \tag{87}$$

in the region of interest. Equation (85) then becomes

$$\mathcal{H} = \frac{T_e + T_i}{T_e' + T_i' + mg/k} \quad . \tag{88}$$

Algabraic manipulation yields

$$\mathcal{H} = \frac{k\left(T_e + T_i\right)/2mg}{k\left(T_e + T_i\right)'/2mg + (1/2)} \quad . \tag{89}$$

Purely as a matter of convenience, I introduce the definitions

$$H = \frac{k\left(T_e + T_i\right)}{2\ mg} \tag{90}$$

(which has been discussed already), and

$$\Gamma = \frac{dH}{dz} \tag{91}$$

and make the simplifying assumption that g is constant. Equation (89) now becomes:

$$\mathcal{H} = \frac{H}{\Gamma + (1/2)} \quad . \tag{92}$$

It is important to note that Eq. (92) embodies no assumptions about T_e and T_i other than those introduced originally. In particular, T_e/T_i is completely arbitrary up to this point. In addition, note that I attach no particular physical significance to the quantity H as used here; it is used for convenience only and serves as an index for (T_e+T_i).

Rearranging Eq. (92) yields

$$\Gamma = \frac{dH}{dz} = \frac{H}{\mathcal{H}} - \frac{1}{2} \quad . \tag{93}$$

The observed data indicate that $\mathcal{H}$ is nearly linear in height. On that basis I make the approximation

$$\mathcal{H} = a + bz \quad , \tag{94}$$

where a and b are determined from the data. Equation (93) now becomes

$$\frac{dH}{dz} = \frac{H}{a+bz} - \frac{1}{2} \quad . \tag{95}$$

By making the transformations $y = z+(a/b)$ and $u = H/y$, the equation becomes homogeneous and may be solved. A solution is given as

$$H = C[z + (a/b)]^{1/b} + \frac{(b/2)}{1-b}[z + (a/b)] \quad , \tag{96}$$

where C is an arbitrary constant. Values can be assigned to the constants by referring to the experimental values shown in Fig. 10. For example, the summer data (Fig. 10a) at 51-deg dip latitude give $\mathcal{H}(500\text{ km}) = 170$ km and $\mathcal{H}(800\text{ km}) = 320$ km. When $z = 0$ corresponds to a height of 500 km, $\mathcal{H}$ can be represented by

$$\mathcal{H} = 170 + 0.5z \quad . \tag{97}$$

Equation (96) now takes a particularly simple form--i.e.,

$$H = C(z + 340)^2 + \frac{1}{2}(z + 340) . \tag{98}$$

To determine an appropriate value for the unknown constant I make use of the observations and theoretical considerations of Hanson in Section III-B. Assume that electron temperature is independent of altitude in this region and that ion temperature increases with increasing altitude, approaching the electron temperature as an upper limit. I can therefore estimate C by requiring that the gradient of ion temperature be either zero or slightly positive at a height of 800 km. This constraint can be stated more explicitly by

$$\Gamma = \frac{dH}{dz} = 2\,C(z + 340) + \frac{1}{2} \tag{99}$$

$$\Gamma(800\text{ km}) = \epsilon = 2\,C(640) + \frac{1}{2}, \qquad 0 \leq \epsilon \tag{100}$$

where $z = 300$ at 800-km height. Then C is found as

$$C = \frac{\epsilon - (1/2)}{1280} . \tag{101}$$

A complete solution to Eq. (93) is now expressed as

$$H = \frac{\epsilon - (1/2)}{1280}(z + 340)^2 + \frac{1}{2}(z + 340) . \tag{102}$$

Solutions to Eq. (102) parametric in ϵ are shown in Fig. 18. The dashed lines represent the maximum value of H for any ϵ. Note that for $\epsilon = 0.5$, there is no maximum to H, and in the region 500 to 800 km., $H = \aleph$. This particular solution is interesting because it is also the solution one would obtain by making the assumption that Γ is constant. This is easily shown by differentiating Eq. (92) with $\partial\Gamma/\partial z = 0$, which gives

$$\frac{d\aleph}{dz} = \frac{1}{2} = \frac{\Gamma}{\Gamma + (1/2)} ; \tag{103}$$

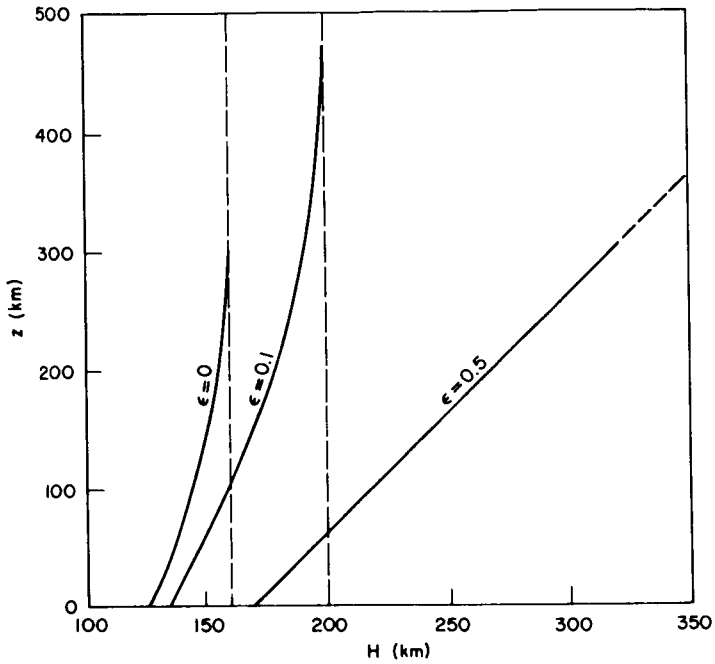

33227

FIG 18. SOLUTIONS TO EQ. (102) FOR THREE VALUES OF ϵ. The parameters are defined as:

$$H = \frac{k\left(T_e+T_i\right)}{2mg} , \qquad \epsilon = \left.\frac{dH}{dh}\right|_{h=800\ km} , \qquad z = 500 + h .$$

For all $\epsilon < 0.5$, H has a maximum; there is no maximum in H for $\epsilon = 0.5$. The dotted lines represent the asymptotic values of H for each ϵ.

hence, $\Gamma = \frac{1}{2}$, and, from Eq. (92);

$$\mathcal{H} = \frac{H}{(1/2) + (1/2)} = H . \tag{104}$$

As stated before, H may be considered as an index to electron-plus-ion temperature. Thus,

$$T_e + T_i = \frac{2mgH}{k} \approx 32H\ ^\circ K . \tag{105}$$

I now make the following assumptions:

$$T_e = \text{constant} \tag{106}$$

$$T_i \leq T_e \tag{107}$$

$$T_i \text{ (maximum)} = T_e \tag{108}$$

$$\epsilon = 0 \ . \tag{109}$$

The solution is plotted in Fig. 19. A solution corresponding to the case $\epsilon = 0.1$ is shown as a dash-dot curve. Comparison of the two curves shows that a small change in ϵ corresponds to a very large change in T_e. The solution for $\epsilon = 0.5$ does not exist in this case since Eq. (108) cannot be satisfied. In order to have a solution for $\epsilon = 0.5$, either or both of the assumptions of Eq. (106) or (107) must be removed.

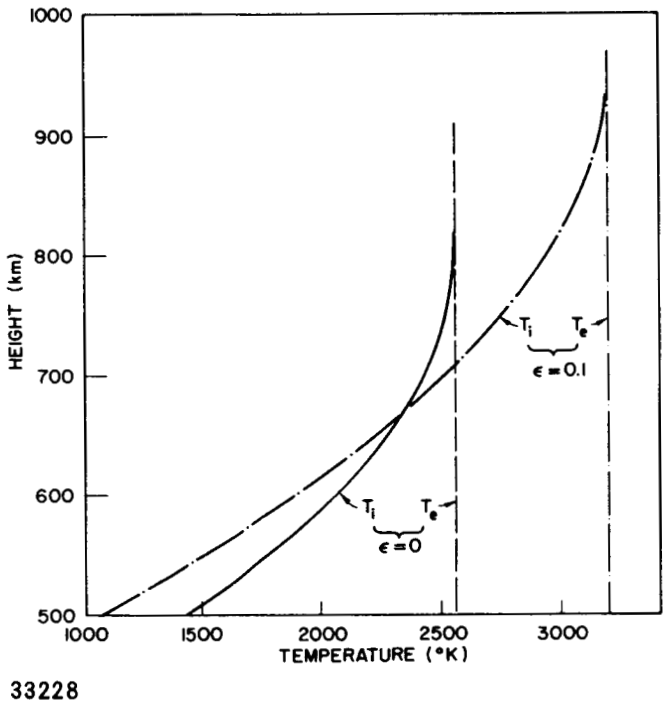

FIG. 19. ION TEMPERATURES AS A FUNCTION OF HEIGHT, AND CONSTANT ELECTRON TEMPERATURE FOR $\epsilon = 0$. The dotted lines represent the solution for $\epsilon = 0.1$. These temperatures correspond to the values of H given in Fig. 18 through the relationship $H = k(T_e+T_i)/2mg$.

The solution for $\epsilon = 0$, can provide profiles of electron and ion temperatures as functions of latitude corresponding to the scale-height profiles of Fig. 10. Since these scale-height profiles are nearly linear in latitude, they can be approximated with straight lines. Applying the methods just described, we obtain the solutions plotted in Fig. 20 for summer daytime and winter daytime conditions respectively.

C. INTERPRETATION OF NIGHTTIME SCALE HEIGHTS

The nighttime data are not as easily interpreted as the daytime data. At the lower latitudes, the results of other workers and the results of my own model suggest that electron and ion temperatures are nearly equal and nearly independent of height. In contrast to this, at the higher latitudes the scale-height profiles are quite similar to daytime profiles for which the analysis of the last section indicates that ion temperatures may not be independent of height. The similarity between the high-latitude nighttime profiles and the daytime profiles suggests that high-latitude electron and ion temperatures can be estimated by the same procedure as used for the daytime analysis. I have performed this analysis for the nighttime data occurring between 69- and 84-deg dip latitude. From Fig. 11 it is evident that such an analysis is not valid below about 69 deg of dip latitude since, in this region, scale-height variations are due primarily to changes in ion constituents. The earlier nighttime analysis at 51 deg dip latitude suggests that values for electron and ion temperature lie between 800 °K and 1000 °K. The transition-level analysis suggests that ion temperatures increase with increasing latitude. I have, therefore, used two different analysis methods for the two different regions and will consider these separately.

1. Midlatitude Analysis. The model developed in Chapter IV was matched to the $\mathcal{H}$ profile given by the 51-deg-dip-latitude nighttime curve in Fig. 9a--i.e., summer data. A comparison of Figs 9a and 9b shows that the 51-deg-dip-latitude nighttime curves are quite similar except that the winter curve is about 100 km lower. The curves are so similar, in fact, that the model yields the same temperatures for each case, and the ion concentrations for each case are simply offset from each other by about 100 km. The results shown in Fig. 14 are thus repeated in Fig. 21, with the summer and winter coordinates shown on opposite sides of the plot.

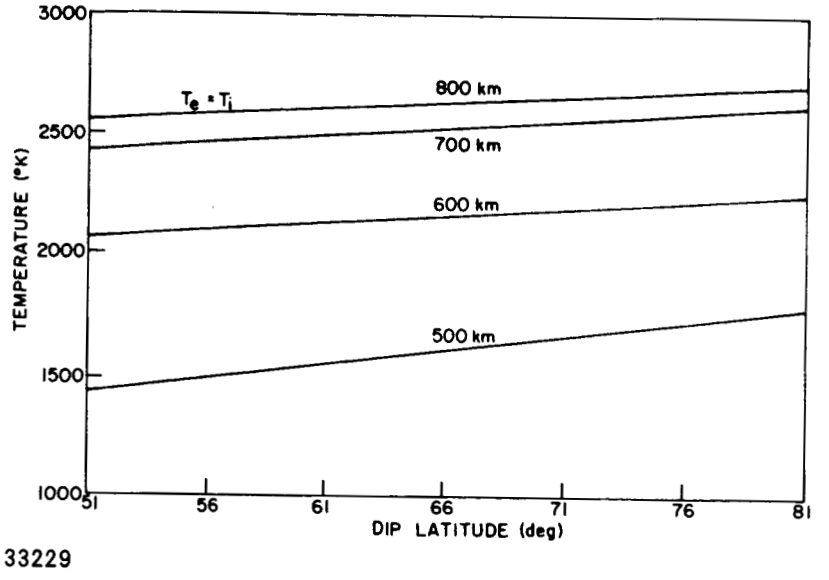

a. Summer, May - July 1963

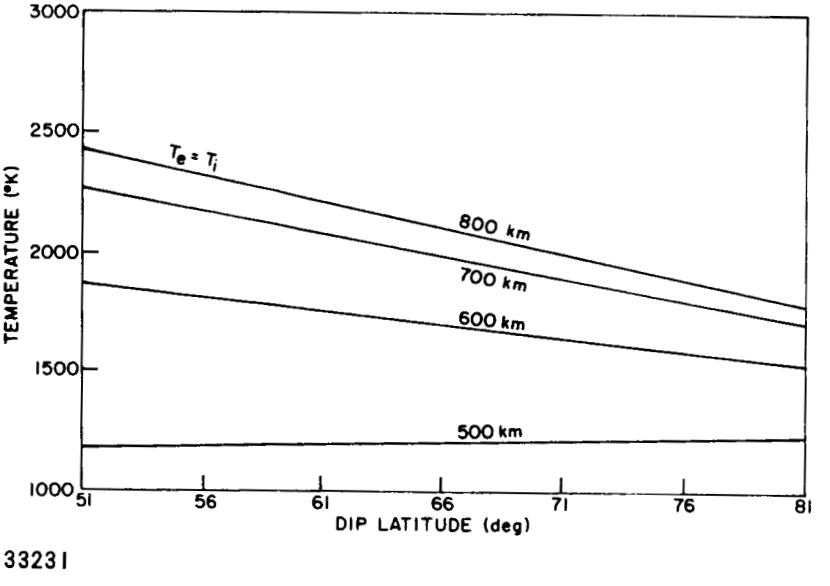

b. Winter, November 1963 - January 1964

FIG. 20. ELECTRON AND ION TEMPERATURES AS FUNCTIONS OF DIP LATITUDE FOR DAYTIME. Electron temperature is assumed everywhere independent of height and is represented by the 800-km curve. Ion temperatures are shown at four heights and $T_e = T_i$ at 800 km.

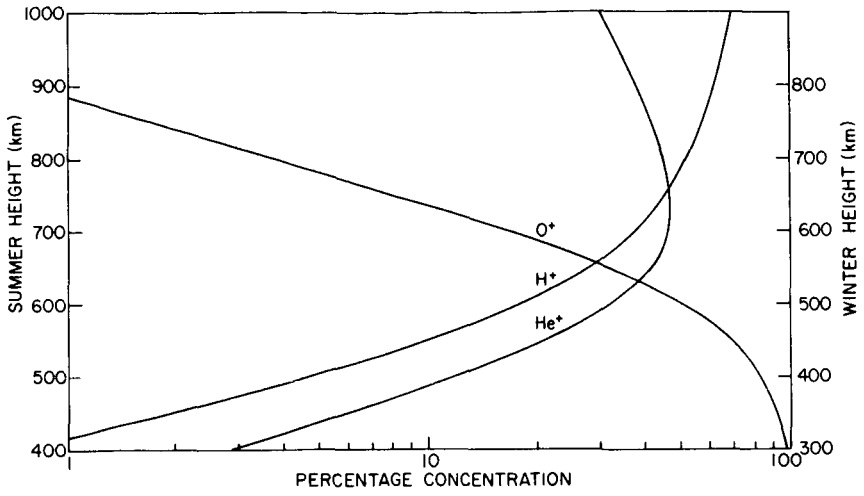

33230

FIG. 21. RELATIVE CONCENTRATIONS OF O^+, He^+, AND H^+ AS FUNCTIONS OF HEIGHT AT 51-DEG DIP LATITUDE FOR NIGHTTIME, SUMMER (MAY - JULY 1963) AND WINTER (NOVEMBER 1963 - JANUARY 1964). The curves are based on a model for which $T_e = T_i = 785\ ^\circ K$.

2. High Latitude Analysis. Here I use the analysis described earlier for use on the daytime profiles. Since at night the $\mathcal{N}$ profiles vary significantly with latitude, the simple form of solution given by Eq. (98) is not adequate. Instead, use Eqs. (94) and (96); thus,

$$\Gamma = \frac{dH}{dz} = \frac{C}{b}\,[z + (a/b)]^{(1-b)/b} + \frac{b/2}{1-b}\ . \tag{110}$$

From the condition $\epsilon = 0$,

$$C = \frac{[(-b/2)/(1-b)]b}{[300 + (a/b)]\ [(1-b)/b]} \tag{111}$$

and

$$H = \left(z + \frac{a}{b}\right)\left(\frac{b/2}{1-b}\right)\ \left\{1 - b\left[\frac{z + (a/b)}{300 + (a/b)}\right]^{(1-b)/b}\right\} \tag{112}$$

where a and b are found, through Eq. (94), from the experimental values of $\mathcal{N}$. The determination of H leads to values for T_e and T_i as described earlier.

Performing the analysis described in 1 and 2 yields values for nighttime temperatures at 51-deg dip latitude and above 69-deg dip latitude. Direct determination of temperatures in between would be difficult because of the lack of precise information on the variation of mean ion mass with latitude. In Fig. 22 are shown the values of electron and ion temperatures as functions of latitude at several altitudes; I have extrapolated from the high-latitude to the midlatitude region with dotted lines.

Comparison of Figs. 22a and 22b shows that, for both summer and winter, temperatures appear to reach a pronounced maximum at between 72- and 75-deg latitude, although summer temperatures appear to be a bit higher. A downward flux of energetic particles from sources such as the solar wind or the Van Allen belts might account for this, although it seems that particles depositing appreciable energy at these altitudes would have to be of fairly low energy. Thus far, the measurement of energetic particle fluxes appears to have been limited to particles with energies greater than about 40 kev.

In addition, from purely geometric considerations, the region above about 70-deg latitude is sunlit nearly all night during the summer period. The summer-night, high-latitude temperatures are thus likely to be the result of both solar flux and whatever heating mechanism is producing the winter conditions. Such an assumption would explain both the higher temperatures during the summer and also the fact that the temperature peaks occur at about 3-deg higher latitude in the summer than in the winter.

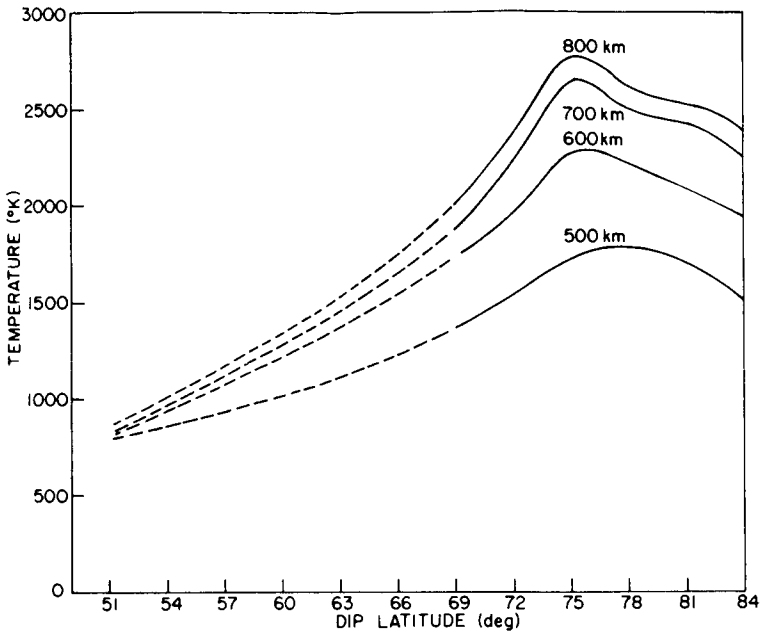

a. Summer, May - July 1963

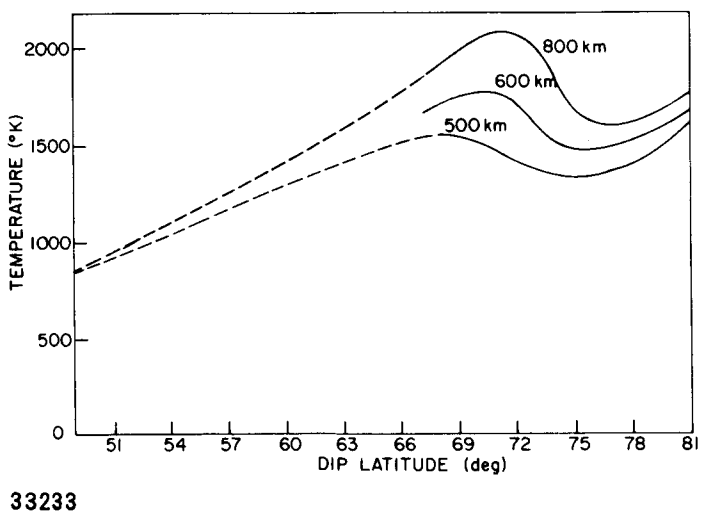

b. Winter, November 1963 - January 1964

FIG. 22. ELECTRON AND ION TEMPERATURES AS FUNCTIONS OF DIP LATITUDE FOR NIGHTTIME. Electron temperature is assumed everywhere independent of height and is represented by the 800-km curve. Ion temperatures are shown at four heights and $T_e = T_i$ at 800 km. Below the 69-deg dip latitude, temperatures are represented approximately by the dotted extensions to the curves.

VIII. THE CONSIDERATION OF A NONZERO FLUX

In Chapter VI I developed the theoretical model for diffusive equilibrium for the case $W = 0$. Now consider the case in which Assumption 4 of Chapter VI is removed--that is, W need not be zero--and the equation of continuity is simply

$$\frac{\partial}{\partial h}(nW) = 0 \ . \tag{113}$$

A velocity introduces an additional term into the force equations. Assuming that the neutral gas is not moving, the diffusion of the ionized particles through the neutral gas results in a viscous drag, which I represent by a term of the form $nm\nu W$, where ν is the collision frequency between the charged particles and the neutrals. The force equations then take the form

$$\frac{\partial}{\partial h}(n_e kT_e) = - n_e m_e g - n_e |e| E - n_e m_e \nu_{en} W_e \tag{114}$$

and

$$\frac{\partial}{\partial h}(n_i kT_i) = - n_i m_i g + n_i |e| E - n_i m_i \nu_{in} W_i \ . \tag{115}$$

If $m_e \nu_{en} \ll m_i \nu_{in}$, $W_e = W_i = W$, and $n_e = n_i = n$, we can add Eqs. (114) and (115) and obtain

$$\frac{\partial}{\partial h}\left[nk\left(T_e + T_i\right)\right] = - n_i m_i g - n_i m_i \nu_{in} W \tag{116}$$

Solving for W results in

$$W = - \frac{1}{m_i \nu_{in}} \left[\frac{1}{n} \frac{\partial}{\partial h}\left(nk\{T_e + T_i\}\right) + m_i g\right] . \tag{117}$$

With some manipulation, this can be put in the form

$$W = - \frac{(1+\tau)kT_i}{m_i \nu_{in}} \left[\frac{1}{n} \frac{\partial n}{\partial h} + \frac{1}{(T_e + T_i)} \frac{\partial}{\partial h} \left(T_e + T_i \right) + \frac{m_i g}{k(T_e + T_i)} \right] . \tag{118}$$

It is convenient to introduce new variables into the problem. Define

$$x = \int_o^h \frac{dh}{H} \tag{119}$$

$$D = \frac{2kT_i}{m_i \nu_{in}} \tag{120}$$

The quantity x is often called the "reduced height." As a corollary to Eq. (119)

$$\frac{\partial}{\partial h} = \frac{1}{H} \frac{\partial}{\partial x} . \tag{121}$$

The quantity D is called a diffusion coefficient. It can be shown that, for the case $T_e = T_i = T$, D is approximately given by

$$D = D_o \exp \left[\left(1 + \frac{3}{2} \Gamma \right) x \right] . \tag{122}$$

According to classical gas kinetic theory, in my simple model of an ionized gas, ν_{in} can be expressed as

$$\nu_{in} \propto nT^{1/2} \tag{123}$$

where n and T are the number density and temperature of the neutrals. Then

$$D \propto \frac{T_i^{1/2}}{n} \propto \frac{T_i^{3/2}}{nT} \tag{124}$$

Since nT varies approximately as exp(-x),

$$D = D_1 T_i^{3/2} \exp(x) \tag{125}$$

$$\frac{\partial D}{\partial h} = \frac{D_1}{H} T_i^{3/2} \exp(x) + \frac{3}{2} D_1 T_i^{1/2} \frac{\partial T_i}{\partial h} \exp(x) \ . \tag{126}$$

Also, since, for $T_e = T_i$,

$$\frac{\partial T_i}{\partial h} = \frac{T_i}{H} \frac{\partial H}{\partial h} = \frac{T_i}{H} \Gamma \ , \tag{127}$$

and then

$$\frac{\partial D}{\partial h} = \frac{1}{H} \frac{\partial D}{\partial x} = \frac{1}{H} \left(1 + \frac{3}{2} \Gamma\right) D \tag{128}$$

from which Eq. (122) follows. Proceeding, if Eqs. (119) - (122) are inserted into Eq. (118),

$$W = - \frac{D}{H} \left[\frac{1}{n} \frac{\partial n}{\partial x} + \Gamma + \frac{1}{2}\right] \ . \tag{129}$$

Using Eqs. (122) and (129), I can formally determine the quantity $\partial(nW)/\partial h$. Then

$$\frac{\partial}{\partial h} (nW) = - \frac{D}{H^2} \left[\frac{\partial^2 n}{\partial x^2} + \frac{3}{2}\left(1+\Gamma+x \frac{\partial \Gamma}{\partial x}\right) \frac{\partial n}{\partial x} + \left(\frac{\partial \Gamma}{\partial x} + \{\Gamma+\frac{1}{2}\}\{1+\frac{1}{2}\Gamma+\frac{3}{2} x \frac{\partial \Gamma}{\partial x}\}\right) n\right]. \tag{130}$$

Setting $\partial(nW)/\partial h = 0$, I obtain the equation

$$\frac{\partial^2 n}{\partial x^2} + \frac{3}{2}\left(1+\Gamma+x \frac{\partial \Gamma}{\partial x}\right) \frac{\partial n}{\partial x} + \left(\frac{\partial \Gamma}{\partial x} + \{\Gamma+\frac{1}{2}\}\{1+\frac{1}{2}\Gamma+\frac{3}{2} x \frac{\partial \Gamma}{\partial x}\}\right) n = 0 \ . \tag{131}$$

A solution to Eq. (131) can be obtained by noting that the statement $\partial(nW)/\partial h = 0$ is equivalent to the statement $nW = \Phi = \text{constant}$. Performing this operating on Eq. (129) leads to

$$\frac{\partial n}{\partial x} + \left(\Gamma+\frac{1}{2}\right)n = -\frac{\Phi H}{D} . \tag{132}$$

Equation (132) can be solved by ordinary linear equation theory. A solution is given as

$$n = C \exp\left[-\int\left(\Gamma+\frac{1}{2}\right)dx\right] + \exp\left[-\int\left(\Gamma+\frac{1}{2}\right)dx\right]\int\exp\left[\int\left(\Gamma+\frac{1}{2}\right)dx\right]\left(-\frac{\Phi H}{D}\right)dx \tag{133}$$

in which C and Φ are arbitrary constants. This complete solution to the general equation is not only very complicated, but also provides little insight into the behavior of scale height with variations in Γ. A great simplification can be made by assuming Γ is constant. Equation (131) then becomes

$$\frac{\partial^2 n}{\partial x^2} + \left(\frac{3}{2} + \frac{3}{2}\Gamma\right)\frac{\partial n}{\partial x} + \left(\Gamma + \frac{1}{2}\right)\left(\frac{1}{2}\Gamma + 1\right) n = 0 , \tag{134}$$

for which the complete solution is:

$$n = A_1 \exp\left[-\left(\Gamma + \frac{1}{2}\right)x\right] + A_2 \exp\left[-\left(\frac{1}{2}\Gamma + 1\right)x\right] . \tag{135}$$

Before proceeding further, it is interesting to note that Eq. (129) can be put in the form:

$$W = \frac{D}{H}\left[\frac{H}{\mathcal{H}} - \left(\Gamma + \frac{1}{2}\right)\right] , \tag{136}$$

then, setting $W = 0$ yields

$$\frac{H}{\mathcal{H}} - \Gamma - \frac{1}{2} = 0 , \tag{137}$$

which is completely equivalent to Eq. (93).

It can be verified by combining the solution of Eq. (135) with Eq. (129) that, for $\Gamma < 1$, an upward (positive) W is associated with a positive coefficient A_2. The coefficient A_1 is associated with the no-flux condition. Values of $\Gamma > 0.3$ are not likely from a physical standpoint, so A_2 must always be positive for an upward flux.

We can operate on Eq. (135) to determine scale height; then

$$\mathcal{H} = \frac{n}{\partial n/\partial h} = - \frac{Hn}{\partial n/\partial x} . \tag{138}$$

Performing this operation on Eq. (135) leads to

$$\mathcal{H}(x) = H(x) \left[\frac{A_1 \exp\{-\left(\Gamma+\frac{1}{2}\right)x\} + A_2 \exp\{-\left(\frac{1}{2}\Gamma+1\right)x\}}{\left(\Gamma+\frac{1}{2}\right) A_1 \exp\{-\left(\Gamma+\frac{1}{2}\right)x\} + \left(\frac{1}{2}\Gamma+1\right) A_2 \exp\{-\left(\frac{1}{2}\Gamma+1\right)x\}} \right] . \tag{139}$$

At $x = 0$ this reduces to

$$\mathcal{H}(0) = H(0) \left[\frac{A_1 + A_2}{\left(\Gamma + \frac{1}{2}\right) A_1 + \left(\frac{1}{2}\Gamma + 1\right) A_2} \right] . \tag{140}$$

The ratio between the scale height at x to the scale height at some reference level can be expressed by dividing Eq. (139) by (140). The definitions

$$R = \frac{\Gamma + 2}{2\Gamma + 1} \tag{141}$$

$$S = \frac{A_2}{A_1} \tag{142}$$

when used with a little algebra, gives the result

$$\frac{\mathcal{H}(x)}{\mathcal{H}(0)} = \frac{H(x)}{H(0)} \left[\frac{(1 + RS)\left(1 + S \exp\{\left(\frac{1}{2}\Gamma - \frac{1}{2}\right)x\}\right)}{(1 + S)\left(1 + RS \exp\{\left(\frac{1}{2}\Gamma - \frac{1}{2}\right)x\}\right)} \right] . \tag{143}$$

By letting the reference height be 500 km and x correspond to 800 km, and by letting $\mathcal{N}(0)$ correspond to an experimental value, say $\mathcal{N}(0) = 170$ km, we can solve Eq. (143) for $\mathcal{N}(x)$ as a function of $H(0)$, using various arbitrary choices for Γ. Equation (141) is solved immediately for any choice of Γ, and S is found from Eq. (140) as

$$S = \frac{[H(0)/\mathcal{N}(0)] - [\Gamma + (1/2)]}{[(\Gamma/2) + 1] - [H(0)/\mathcal{N}(0)]} . \tag{144}$$

Values for x are found from Eq. (119)

$$x = \int_0^{300} \frac{dh}{H} = \int_0^{300} \frac{dh}{H(0) + \Gamma h} = \frac{1}{\Gamma} \ln \left[\frac{H(0) + 300\,\Gamma}{H(0)}\right] \tag{145}$$

if $\Gamma \neq 0$, and

$$x = \frac{300}{H} \tag{146}$$

if $\Gamma = 0$. Solutions to Eq. (143) are shown in Fig. 23. Included in the figure are values of $\mathcal{N}(x)/\mathcal{N}(0)$ corresponding to the summer and winter daytime experimental values. Superimposed on the Γ curves--i.e., solutions to Eq. (143)--are $W(0)$ curves, representing various solutions to Eq. (136). The intersection of any two curves represents a simultaneous solution to Eqs. (136) and (143). For any assumed value for Γ, one can thus observe the effect on $\mathcal{N}(x)/\mathcal{N}(0)$ of variations in $W(0)$; conversely, for any assumed value for $W(0)$, one can observe the effect on $\mathcal{N}(x)/\mathcal{N}(0)$ of variations in Γ. The derivation of a numerical expression for diffusion velocity is now considered, and this expression provides the source for the numerical values of the various $W(0)$ curves. If

$$F = \frac{H}{\mathcal{N}} - \Gamma - \frac{1}{2} \tag{147}$$

then, from Eq. (136),

$$W = \frac{DF}{H} . \tag{148}$$

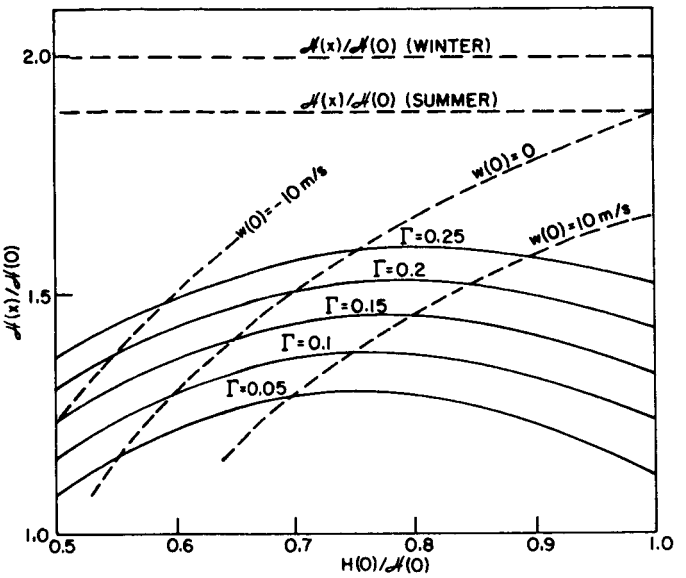

33234

FIG. 23. GRAPHIC SIMULTANEOUS SOLUTIONS TO EQS. (136) AND (143). The ordinate is $\mathcal{H}(800\text{ km})/\mathcal{H}(500\text{ km})$, a quantity that is available as experimental data. The abscissa is $H(500\text{ km})/\mathcal{H}(500\text{ km})$, where H is defined as $H = k(T_e+T_i)/2mg$ km. The parameter Γ is defined as $\Gamma = dH/dh$, (km km) assumed constant--i.e., $d\Gamma/dh = 0$. The parameter $W(0)$ is defined as an upward diffusion velocity at a height of 500 km, associated with a nondivergent flux. The dashed lines at the top of the figure represent experimentally determined daytime values $\mathcal{H}(800\text{ km})/\mathcal{H}(500\text{ km})$ at 51-deg dip latitude for summer (May - July 1963) and winter (November 1963 - January 1964).

Quinn and Nisbet (1965) have experimentally determined a value for the nighttime diffusion coefficient to be:

$$D = \frac{(0.5 \pm 0.3)\ T^{1/2} \times 10^{17}}{n(0)}\ \text{cm}^2\ \text{sec}^{-1}\ . \qquad (149)$$

If Eq. (149) is also approximately true during the day, one can make estimates of T and $n(0)$ and thus determine W. O'Sullivan et al (1963), using drag data from the Explorer IX Satellite, deduced atmospheric density to be 2×10^{-15} gm/cm^3 at an altitude of 500 km. Estimating a mean neutral mass of 16 amu corresponding to a predominance of atomic oxygen, one easily obtains

$$n(0) = 7.5 \times 10^7\ \text{cm}^{-3} \quad \text{at 500 km}\ . \qquad (150)$$

A reasonable assumption for daytime average temperature of neutrals is $T = 1300\ ^{\circ}K$. When these values are inserted into Eq. (149),

$$D = \frac{(0.5)(1300)^{1/2} \times 10^{17}}{7.5 \times 10^{7}} = 2.4 \times 10^{10}\ cm^{2} sec^{-1} \quad . \qquad (151)$$

Use of a typical value of $H = 140$ km based on my assumptions about electron and ion temperatures, yields

$$W = 17\ F \text{ meters sec}^{-1} \quad , \qquad (152)$$

which becomes

$$W(0) = 17\ \frac{H(0)}{\mathcal{N}(0)} - \Gamma - \frac{1}{2} \quad . \qquad (153)$$

For any assumed value of $W(0)$ one obtains a unique relationship between $H(0)/\mathcal{N}(0)$ and Γ, which permits plotting familes of $W(0)$ curves.

It can be seen that, under the assumptions made here--i.e., Γ = constant--a given value of $\mathcal{N}(x)/\mathcal{N}(0)$ is nearly independent of $W(0)$. On the other hand, for a given experimental value of $\mathcal{N}(x)/\mathcal{N}(0)$ and an assumed value for Γ, $W(0)$ and $H(0)/\mathcal{N}(0)$ are almost linearly related. From this it can be seen that estimates of electron and ion temperature lead to estimates of drift velocities. The values of temperatures and temperature gradients suggested by the results of Evans (see Fig. 5) yield approximate values of

$$\frac{H(0)}{\mathcal{N}(0)} = 0.64 \qquad (154)$$

and

$$\Gamma \geq 0.1 \quad , \qquad (155)$$

for which $W(0) \leq 3$ m/sec.

It should be pointed out that all of this analysis following Eq. (133) has been based on the serious approximation that Γ = constant, which is necessary in order to make the expressions tractable. I have already pointed out the consequences of making such an assumption: the temperatures resulting from such an analysis tend to be larger than seems reasonable. The usefulness of these results must be limited to the following:

1. For any particular temperatures and temperature gradients, $\mathcal{H}$ and W are nearly independent.
2. From consideration of reasonable values of temperatures and temperature gradients, typical drift velocities must be less than, say, 10 m/sec at 500 km. For typical electron density of $10^5/cm^3$ at 500 km, such velocities would lead to a flux of less than 10^8 cm^{-2} sec^{-1}.

IX. CONCLUSIONS AND RECOMMENDATIONS

The analysis of scale heights of the topside ionosphere I developed in the present research can lead to determination of electron and ion temperature distributions and relative ion concentrations. I have used this method to study the diurnal, spatial, and seasonal variations of these quantities, and my results are shown in Figs. 16 through 22.

These parameters in the region under consideration can be adequately interpreted within the assumption that the ionosphere is in diffusive equilibrium. A useful property of a diffusive equilibrium mixture of ionized gases is that the transition from dominance by one ion to dominance by another is a narrow, well defined region, and this transition causes a sharp inflection in the scale-height profile. The transition level of $(O^+ - He^+, H^+)$ ions studied was found to vary both with latitude and with time. In particular, at high latitudes and in the daytime, the transition level is so high that it can be assumed that O^+ dominates, thus permitting the interpretation of scale heights entirely in terms of temperature variations.

The results of this study of the possibility of nonzero flux, plus the results of other workers, are consistent with an upward flux of no greater than 10^8 cm^{-2} sec^{-1}, at least for the assumption of a constant gradient of temperature with height.

In general, however, the assumption that temperature variations with height are linear can lead to large errors in temperature.

It would certainly be a worthwhile effort to develop a method for effectively reducing the ionogram data for heights above 800 km. An increase of even 200 km in the upper limit of the data would greatly improve the accuracy of the model, as well as extend our knowledge of the diurnal variation of the transition level.

Arbitrary temperature variation in the nonzero-flux problem should be studied. Since the expressions in this problem are not tractable analytically, such a study would require numerical procedures.

APPENDIX A. DETERMINATION OF SCALE-HEIGHT PROFILES FROM ALOUETTE SOUNDINGS

The reduction of ionograms to electron density profiles are discussed in Thomas and Westover (1963), Thomas, Long, and Westover (1963), and Thomas et al (1964). I present here a brief description of the earlier method--that of Thomas and Westover. The later methods are improved and slightly more complicated versions of the one outlined here and not fundamentally different.

For any transmitted pulse of a particular frequency, the virtual depth of penetration into the plasma can be expressed as

$$h' = \int_o^h \mu' \, dh \qquad (A.1)$$

where h and h' are the real and virtual depth respectively of the point of reflection measured from the satellite, and μ' is the group refractive index.

Thomas and Westover assume that h can be expressed as a polynomial in $f_p - f_o$, where f_p is the plasma frequency at depth h and f_o is the plasma frequency at the satellite. Then

$$h = \sum_{j=1}^{n} \alpha_j (f_p - f_o)^j \; . \qquad (A.2)$$

Since (A.2) is assumed to be true for all values of h, then it is true at any particular value $h = h_i$. Equation (A.2) can thus be restated as

$$h_i = \sum_{j=1}^{n} \alpha_j \, (f_i - f_o)^j \; . \qquad (A.3)$$

We can express Eq. (A.3) for a series of different h_i's. If (A.3) is expressed for n different values of h_i, the equation can be put into matrix form:

$$\begin{vmatrix} h_1 \\ h_2 \\ \cdot \\ \cdot \\ \cdot \\ h_n \end{vmatrix} = \begin{vmatrix} (f_1-f_o) & (f_1-f_o)^2 & \cdots & (f_1-f_o)^n \\ (f_2-f_o) & (f_2-f_o)^2 & \cdots & \\ \cdot & \cdot & & \cdot \\ \cdot & \cdot & & \cdot \\ \cdot & \cdot & & \cdot \\ (f_n-f_o) & (f_2-f_o)^2 & \cdots & (f_n-f_o)^n \end{vmatrix} \begin{vmatrix} \alpha_1 \\ \alpha_2 \\ \cdot \\ \cdot \\ \cdot \\ \alpha_n \end{vmatrix} . \qquad (A.4)$$

This can also be expressed in symbolic form as

$$\underline{h} = \underline{A}\,\underline{\alpha} \qquad (A.5)$$

where $\underline{A}$ is an n matrix with a typical element

$$A_{jk} = (f_j-f_o)^k . \qquad (A.6)$$

Equation (A.1) can be developed in the same manner. For any particular $h' = h_i'$,

$$h_i' = \int_o^{h_i} \mu'\, dh = \int_{f_o}^{f_i} \mu' \frac{dh}{df_p}\, df_p . \qquad (A.7)$$

Differentiating Eq. (A.2) and combining with (A.7) yields

$$\frac{dh}{df_p} = \sum_{j-1}^{n} j\,\alpha_j (f_p-f_o)^{j-1} \qquad (A.8)$$

and

$$h_i' = \sum_{j-1}^{n} \alpha_j \int_{f_o}^{f_i} \mu' \; j(f_p - f_o)^{j-1} \, df_p \; . \tag{A.9}$$

Expressing Eq. (A.9) for a series of n different values of h_i' gives

$$\begin{vmatrix} h_1' \\ h_2' \\ \cdot \\ \cdot \\ \cdot \\ h_n' \end{vmatrix} = \begin{vmatrix} \int_{f_o}^{f_1} \mu' df_p & \int_{f_o}^{f_1} 2\mu'(f_1 - f_o) df_p & \cdots & \int_{f_o}^{f_1} n\mu'(f_1 - f_o)^{n-1} \, df_p \\ \int_{f_o}^{f_2} \mu' df_p & \int_{f_o}^{f_2} 2\mu'(f_2 - f_o) df_p & \cdots & \\ \cdot & \cdot & \cdot & \cdot \\ \cdot & \cdot & \cdot & \cdot \\ \cdot & \cdot & \cdot & \cdot \\ \int_{f_o}^{f_n} \mu' df_p & & \cdots & \int_{f_o}^{f_n} n\mu'(f_n - f_o)^{n-1} \, df_p \end{vmatrix} \begin{vmatrix} \alpha_1 \\ \alpha_2 \\ \cdot \\ \cdot \\ \cdot \\ \alpha_n \end{vmatrix} \tag{A.10}$$

or in symbolic form as

$$\underline{h}' = \underline{B} \, \underline{\alpha} \tag{A.11}$$

where $\underline{B}$ is an n-by-n matrix with a typical element

$$B_{jk} = \int_{f_o}^{f_j} k\mu'(f_j - f_o)^{k-1} \, dp \; . \tag{A.12}$$

Combining Eqs. (A.11) and (A.5) yields

$$\underline{h} = \underline{A} \, \underline{B}^{-1} \, \underline{h}' = \underline{C} \, \underline{h}' \tag{A.13}$$

where $\underline{C}$ is an n-by-n matrix that depends only on f_0, f_i, and μ'.

Since f_0 is known from the ionogram and the various f_i are chosen, only μ' needs yet be expressed in order to have a complete solution to Eq. (A.1). It should be noted in passing, however, that the matrix operation expressed in Eq. (A.13) requires that $\underline{A}$ and $\underline{B}$ be square matrices. In other words, the order of the assumed polynomial has to be the same as the number of values for h_i and h_i', which are chosen.

Group refractive index is a straightforward, though complicated function given by

$$\mu' = \frac{d}{df}(f\mu) \tag{A.14}$$

where, for a propagating plane wave,

$$\mu^2 = 1 - \left(\frac{2f_p^2}{f^2}\right)\left\{\frac{2-\left(f_t^2/f^2\right)}{1-\left(f_p^2/f^2\right)} \pm \left[\frac{f_t^2/f^2}{1-\left(f_p^2/f^2\right)} + \frac{4f_l^2}{f^2}\right]^{1/2}\right\}^{-1} \tag{A.15}$$

Equation (A.15) is simply the Appleton-Hartree equation for propagation through an ionized medium. The parameters are:

$$f_t = \frac{eB}{m}\sin\theta \tag{A.16}$$

$$f_l = \frac{eB}{m}\cos\theta \tag{A.17}$$

$$f_p^2 = \frac{N e^2}{4\pi^2 \epsilon_o m} \tag{A.18}$$

where θ is the angle between the propagating wave normal and the magnetic-field vector, and f is the wave frequency. In practice, and for an as yet unexplained reason, the ordinary mode trace observed on the ionograms is incomplete; it does not appear for small virtual depths. For this reason, the extra-ordinary mode is used, which corresponds to the choice of the minus sign in Eq. (A.15).

The use of the extraordinary wave also requires an indirect determination of the integration limits f_o and f_i, since they cannot be determined directly. The extraordinary-wave reflection conditions are given as

$$f_o^2 = f_{xv}^2 - f_{xv} f_{Hv} \tag{A.19}$$

$$f_i^2 = f_{xi}^2 - f_{xi} f_{Hi} \tag{A.20}$$

where f_{xv} and f_{Hv} are the extraordinary-wave frequency and electron gyro frequency at the vehicle, and f_{xi} and f_{Hi} are the same parameters at the point of reflection. From Eqs. (A.19) and (A.20), values for f_o and f_i may be determined.

Corresponding to every value of f_i, a value of h_i' has been measured and a value of h_i has been computed. Since $f_i = f_p$ at $h = h_i'$, then, from Eq. (A.18),

$$N(h=h_i) = N(f_p=f_i) = \frac{2\pi f_i (\epsilon_o m)^{1/2}}{e} . \tag{A.21}$$

Thus $N(h)$ has been determined at a series of depths below the satellite.

The values of $h = h_i$ for which $N(h)$ is determined are not in general equally spaced, even when equal frequency intervals are chosen. However, h is still given by the polynomial of Eq. (A.2), which is constrained to pass through the points $h = h_i$ at $f = f_i$; h is thus defined continuously and can be found for arbitrary wave frequencies.

APPENDIX B. THE COMPUTER PROGRAM FOR DETERMINING M

It is instructive to consider the method used to find numerical values for $M(z)$ by use of a digital computer. In the most general case, M is most easily solved from Eqs. (70) and (77), which are repeated here for reference.

$$M(z) = \frac{2}{g} \frac{\tau\left(\sum_i n_i m_i g + n_e k T_i'\right) - n_e k T_e'}{n_e(1+\tau)} \tag{B.1}$$

$$\frac{n_{eo} T_{eo}}{T_e} \exp\left[-\int_o^z \frac{Mg}{2kT_e}\, dh\right] = \frac{T_{io}}{T_i} \sum_i n_{io} \exp\left[\int_o^z \frac{(M-2m_i)g}{2kT_i}\, dh\right] \tag{B.2}$$

In solving these equations, I make the following assumptions:

1. All densities and temperatures are known at the reference level.
2. The altitude variations of T_e and T_i are known.

From Assumptions 1 and 2, it is seen that $M(0)$ can be found immediately. The functional forms of temperature used are the simplest possible to describe gradients:

$$T_e = T_{eo}\,[1 + (A_e)\, z] \tag{B.3}$$

and

$$T_i = T_{io}\,[1 + (A_i)\, z] \tag{B.4}$$

where A_e and A_i can be assigned different values. Equation (B.1) can be put into a more convenient form for the present use. By algebraic manipulation,

$$M(z) = \frac{2T_e}{T_e + T_i}\left[\frac{\sum_i n_i m_i}{\sum_i n_i} + \frac{kT_i}{g}\left(\frac{T_i'}{T_i} - \frac{T_e'}{T_e}\right)\right]. \tag{B.5}$$

By differentiating Eqs. (B.3) and (B.4) and substituting into Eq. (B.5), we can solve for $M(0)$ thus:

$$M(0) = \frac{2T_{eo}}{T_{eo}+T_{io}} \left[\frac{\sum_i n_{io} m_i}{\sum_i n_{io}} + \frac{kT_{io}}{g(0)} (A_i - A_e) \right] . \qquad (B.6)$$

For any chosen values of A_i and A_e, we have an explicit value for $M(0)$.

Next assume that, for all cases of interest, M is a slowly varying function, so that it can be closely approximated by straight-line segments over reasonable distances.

If the entire range of z, $(z_{min} \leq z \leq z_{max})$ is divided into segments of length Δh, then $z = N\Delta h$, where N is an integer of value $z_{min}/\Delta h \leq N \leq z_{max}/\Delta h$. We can solve for M for successive values of N and designate the solutions as $M(N)$. Since $M(0)$ is already known from Eq. (B.6), we can solve Eq. (B.2) for $M(1)$, $M(2)$, etc.

1. Case 1, N = 1

Then the variables take the following form:

$$z = \Delta h \qquad (B.7)$$

$$g = \frac{g(0)\, R_o^2}{R^2} = \frac{g(0)\, R_o^2}{[R_o + (\Delta h/2)]^2} \qquad (B.8)$$

$$\left.\begin{aligned} T_e &= T_{eo} (1 + A_e \Delta h/2) \qquad (B.9) \\ T_i &= T_{io} (1 + A_i \Delta h/2) \qquad (B.10) \end{aligned}\right\} \text{ Inside the integrals}$$

$$\left.\begin{aligned} T_e &= T_{eo} (1 + A_e \Delta h) \qquad (B.11) \\ T_i &= T_{io} (1 + A_i \Delta h) \qquad (B.12) \end{aligned}\right\} \text{ Outside the integrals}$$

$$M = \frac{M(0) + M(1)}{2} \qquad (B.13)$$

$$\int_o^z \frac{Mg}{2kT_e}\,dh = \frac{g(0)\,R_o^2}{2k}\left\{\frac{[M(0)+M(1)]\,\Delta h}{2T_{eo}[1+A_e(\Delta h/2)][R_o+(\Delta h/2)]^2}\right\} \qquad (B.14)$$

$$\int_o^z \frac{(M-2m_i)g}{2kT_i}\,dh = \frac{g(0)\,R_o^2}{2k}\left\{\frac{[M(0)+M(1)-4m_i]\,\Delta h}{2T_{io}[1+A_i(\Delta h/2)][R_o+(\Delta h/2)]^2}\right\}. \qquad (B.15)$$

Substituting Eqs. (B.14) and (B.15) into Eq. (B.2) and rearranging yields

$$n_{eo}\,\frac{1+A_i\Delta h}{1+A_e\Delta h}\,\exp\left[-\frac{g(0)\,R_o^2}{2k}\left\{\frac{[M(0)+M(1)]\,\Delta h}{2T_{eo}[1+A_e(\Delta h/2)][R_o+(\Delta h/2)]^2}\right\}\right]$$

$$=\sum_i n_{io}\,\exp\left[\frac{g(0)\,R_o^2}{2k}\left\{\frac{[M(0)+M(1)-4m_i]\,\Delta h}{2T_{io}[1+A_i(\Delta h/2)][R_o+(\Delta h/2)]^2}\right\}\right]. \qquad (B.16)$$

Equation (B.16), although transcendental, can certainly be solved for a numerical value of $M(1)$, since everything else is known.

2. Case 2, $N = 2$

Then

$$\int_o^z \frac{Mg}{2kT_e}\,dh = \int_o^{\Delta h} \frac{Mg}{2kT_e}\,dh + \int_{\Delta h}^{2\Delta h} \frac{Mg}{2kT_e}\,dh \qquad (B.17)$$

$$\int_o^z \frac{(M-2m_i)g}{2kT_i}\,dh = \int_o^{\Delta h} \frac{(M-2m_i)g}{2kT_i}\,dh + \int_{\Delta h}^{2\Delta h} \frac{(M-2m_i)g}{2kT_i}\,dh\,. \qquad (B.18)$$

The integrals from zero to Δh are known from Eqs. (B.14), (B.15), and (B.16), so that Eqs. (B.17) and (B.18) can be expressed as:

$$\int_o^z \frac{Mg}{2kT_e}\,dh = \int_o^{\Delta h} \frac{Mg}{2kT_e}\,dh + \frac{g(0)\,R_o^2}{2k}\left\{\frac{[M(1) + M(2)]\,\Delta h}{2T_{eo}[1+A_e(3\Delta h/2)][R_o+(3\Delta h/2)]^2}\right\} \tag{B.19}$$

and

$$\int_o^z \frac{(M-2m_i)g}{2kT_i}\,dh = \int_o^{\Delta h} \frac{(M-2m_i)g}{2kT_i}\,dh + \frac{g(0)\,R_o^2}{2k}\left\{\frac{[M(1) + M(2) - 4m_i]\,\Delta h}{2T_{io}[1+A_i(3\Delta h/2)][R_o+(3\Delta h/2)]^2}\right\}. \tag{B.20}$$

As before, these equations can be substituted into Eq. (B.2), and $M(2)$ can be found explicitly, since everything else is known. It is easily seen how this computation can be put on a routine basis for both positive and negative values of N. Thus we can describe a complete profile of $M(z)$ by evaluating M at discreet points $z = N\Delta h$. At every point where $M(z)$ is defined, we can also determine values of $\mathcal{H}(z)$ through the various equations that have already been described.

For anyone who might consider making such a computation, it should be noted that the computation represented by equation (B.2) is essentially a differentiation combined with a continuous extrapolation, and as such it is subject to undamped oscillations, particularly where the function $M(z)$ is required to have its slope change significantly in the space of one Δh interval. Such a problem can be eliminated by making the intervals sufficiently short. For the present problem, an interval of 10 km was found to be satisfactory.

APPENDIX C. RECENT ALOUETTE SATELLITE DATA

Since this report was written, a small quantity of additional data has become available from the Defence Research Board Telecommunications Establishment of Canada. The additional data consist of tabulated values of electron density as a function of height obtained from the Alouette satellite. The data were obtained during the period October through December 1962 and from several receiving stations. Since these data were obtained through a completely different reduction method than that described in Appendix A, it is interesting to compare corresponding results obtained through the two methods. The curves in Fig. 24 show scale height as a function of dip latitude obtained from two daytime passages for which data were obtained in this latitude region. These curves are seen to agree reasonably well with those of Fig. 10b.

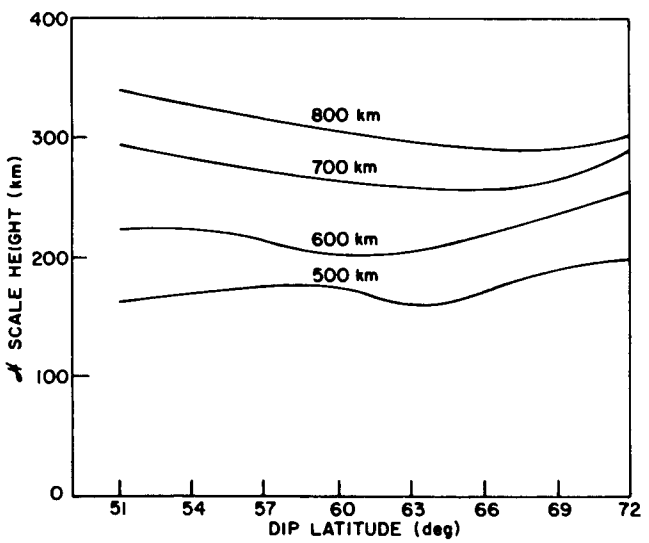

33235

FIG. 24. WINTER DAYTIME SCALE HEIGHT AS A FUNCTION OF DIP LATITUDE AT A SERIES OF ALTITUDES. These curves represent the data from two Alouette passages recorded and analyzed by DRBTE of Canada.

BIBLIOGRAPHY

1. Angerami, J. J., and J. O. Thomas, "Studies of Planetary Atmospheres," J. Geophys. Res., 69, 1964, p. 4537.

2. Barrington, R. E., J. S. Belrose, and G. L. Nelms, "Ion Composition and Temperatures at 1000 Km as Deduced from Simultaneous Observations of a VLF Plasma Resonance and Topside Sounding Data in the Alouette I Satellite," J. Geophys. Res., 70, 1965, p. 1647.

3. Bates, D. R., "Charge Transfer and Ion-Atom Interchanging Collisions," Proc. Phys. Soc., A68, 1954, p. 344.

4. Bates, D. R. and H. S. W. Massey, "The Basic Reactions in the Upper Atmosphere," Proc. Roy. Soc., A192, 1947, p. 1.

5. Bourdeau, R. E., and S. J. Bauer, "Structure of the Upper Atmosphere Deduced drom Charged Particle Measurements on Rockets and the Explorer VIII Satellite," Space Research III, John Wiley & Sons, Inc., New York, May 1962, p. 173.

6. Bourdeau, R. E., and J. L. Donley, "Explorer VIII Satellite Measurements in the Upper Ionosphere," Proc. Roy. Soc., A281, 1964, p. 514.

7. Bowen, P. J., et al, "Ion Composition of the Upper F Region," Proc. Roy. Soc., A281, 1964, p. 504.

8. Brace, L. H., and N. W. Spencer, "First Electrostatic Probe Results from Explorer 17," J. Geophys. Res., 69, 1964, p. 4686.

9. Brace, L. H., N. W. Spencer, and G. R. Carignan, "Ionosphere Electron Temperature Measurements and their Implications," J. Geophys. Res., 68, 1963, p. 5397.

10. C. D. R. T. E., "Alouette, Satellite 1962 Beta Alpha One," published by the Canadian Defence Research Board, Ottawa, 1962.

11. Chapman, S., "The Absorption and Dissociative or Ionizing Effect of Monochromatic Radiation in an Atmosphere on a Rotating Earth," Proc. Phys. Soc., 43, 1931, p. 26.

12. Dalgarno, A., M. McElroy, and R. Moffett, "Electron Temperatures in the Ionosphere," Plan. Space Sci., 11, 1963, p. 463.

13. Dungey, J. W., "Electrodynamics of the Outer Atmosphere," Report of the Physical Society Conference at Cavendish Laboratory, Cambridge, published by the Physical Society, London, Sep 1954, p. 229.

14. Evans, J. V., and M. Loewenthal, "Ionospheric Backscatter Observations," Plan. Space Sci., 12, 1964, p. 915.

15. Ferraro, V. C. A., "Diffusion of Ions in the Ionosphere," Terrestrial Magnetism and Atmospheric Electricity, 50, 1945, p. 215.

16. Hanson, W. B., "Electron Temperatures in the Upper Atmosphere," Space Research III, John Wiley & Sons, Inc., New York, May 1962, p. 282.

17. Hanson, W. B., and T. N. L. Patterson, "The Maintenance of the Night-Time F-Layer," Plan. Space Sci., 12, 1964, p. 979.

18. Hulburt, E. O., "Ionization in the Upper Atmosphere of the Earth," Phys. Rev., 31, 1928, p. 1018.

19. Johnson, C. Y., E. B. Meadows, and J. C. Holmes, "Ion Composition of the Arctic Ionosphere," J. Geophys. Res., 63, 1958, p. 443.

20. King, J. W., et al, "Preliminary Investigation of the Structure of the Upper Ionosphere as Observed by the Topside Sounder Satellite, Alouette," Proc. Roy Soc., A281, 1964, p. 464.

21. Mange, P., "The Distribution of Minor Ions in Electrostatic Equilibrium in the High Atmosphere," J. Geophys. Res., 65, 1960, p. 3833.

22. McIlwain, C. E., "Coordinates for Mapping the Distribution of Magnetically Trapped Particles," J. Geophys. Res., 66, 1961, p. 3681.

23. Nicolet, M., "Helium, an Important Constituent in the Lower Exosphere," J. Geophys. Res., 66, 1961, p. 2263.

24. Nicolet, M., and P. Mange, "The Dissociation of Oxygen in the High Atmosphere," J. Geophys. Res., 59, 1954, p. 15.

25. Nier, A. O., et al, "Neutral Composition of the Atmosphere in the 100-to-200-kilometer Range," J. Geophys. Res., 69, 1964, p. 979.

26. Onwumechilli, A., "The Effective Equator for Geomagnetic Sq. Variations," J. Geophys. Res., 69, 1964, p. 5063.

27. O'Sullivan, W. J., Jr., C. W. Coffee, Jr., and G. M. Keating, "Air Density Measurements from the Explorer IX Satellite," Space Research III, John Wiley & Sons, Inc., New York, May 1962, p. 89.

28. Paul, A. K., and J. W. Wright, "Electron Density Profile Analysis of Topside Sounder Ionograms," J. Geophys. Res., 69, 1964, p. 1431.

29. Quinn, T. P., and J. S. Nisbet, "Recombination and Transport in the Nighttime F Layer of the Ionosphere," J. Geophys. Res., 70, 1965, p. 113.

30. Ratcliffe, J. A., Physics of The Upper Atmosphere, Academic Press, New York, 1960, p. 441.

31. Schaefer, E. J., and J. Brown, "Additional Rocket-Borne Mass Spectrometer Measurements of the Dissociation of Oxygen," J. Geophys. Res., 69, 1964, p. 1455.

32. Shimazaki, T., "Nighttime Variations of F-Region Electron Density Profiles at Puerto Rico," J. Geophys. Res., 69, 1964, p. 2781.

33. Thomas, J. O., "The Electron Density Distribution in the F_2 Layer of the Ionosphere in Winter," J. Geophys. Res., 68, 1963, p. 2707.

34. Thomas, J. O., B. R. Briggs, L. Colin, M. J. Rycroft, and M. Covert, "Digital Computer Programs for the Reduction of Alouette I Topside Ionograms to Electron Density Profiles," Ames Research Center (NASA), Oct 1964.

35. Thomas, J. O., A. R. Long, and D. Westover, "The Calculation of Electron Density Profiles from Topside Sounder Records," J. Geophys. Res., 68, 1963, p. 3237.

36. Thomas, J. O., and A. Y. Sader, "Electron Density at the Alouette Orbit," J. Geophys. Res., 69, 1964, p. 4561.

37. Thomas, J. O., and D. Westover, "The Calculation of Electron Density Profiles from Topside Ionograms Using a Digital Computer," Rept. SEL-63-130 (TR 5), Stanford Electronics Laboratories, Stanford, Calif., Aug 1963.

38. Warren, E. S., "Sweep Frequency Radio Soundings of the Topside of the Ionosphere," Canadian J. Phys., 40, 1962, p. 1692.

39. Yonezawa, T., "A New Theory of Formation of the F_2 Layer," J. Radio Res. Labs., 3, 1956, p. 1.